

Article

Evaluation of the Prolate Spheroidal Wavefunctions via a Discrete-Time Fourier Transform Based Approach

Natalie Baddour *  and Zuwen Sun 

Department of Mechanical Engineering, University of Ottawa, 161 Louis Pasteur, Ottawa, ON K1N 6N5, Canada; zsun046@uottawa.ca

* Correspondence: nbaddour@uottawa.ca

Abstract: Computation of prolate spheroidal wavefunctions (PSWFs) is notoriously difficult and time consuming. This paper applies operator theory to the discrete Fourier transform (DFT) to address the problem of computing PSWFs. The problem is turned into an infinite dimensional matrix operator eigenvalue problem, which we recognize as being the definition of the DPSSs. Truncation of the infinite matrix leads to a finite dimensional matrix eigenvalue problem which in turn yields what is known as the Slepian basis. These discrete-valued Slepian basis vectors can then be used as (approximately) discrete time evaluations of the PSWFs. Taking an inverse Fourier transform further demonstrates that continuous PSWFs can be reconstructed from the Slepian basis. The feasibility of this approach is shown via theoretical derivations followed by simulations to consider practical aspects. Simulations demonstrate that the level of errors between the reconstructed Slepian basis approach and true PSWFs are low when the orders of the eigenvectors are low but can become large when the orders of the eigenvectors are high. Accuracy can be increased by increasing the number of points used to generate the Slepian basis. Users need to balance accuracy with computational cost. For large time-bandwidth product PSWFs, the number of Slepian basis points required increases for a reconstruction to reach the same error as for low time-bandwidth products. However, when the time-bandwidth products increase and reach maximum concentration, the required number of points to achieve a given error level achieves steady state values. Furthermore, this method of reconstructing the PSWF from the Slepian basis can be more accurate when compared to the Shannon sampling approach and traditional quadrature approach for large time-bandwidth products. Finally, since the Slepian basis represents the (approximate) sampled values of PSWFs, when the number of points is sufficiently large, the reconstruction process can be omitted entirely so that the Slepian vectors can be used directly, without a reconstruction step.

Keywords: PSWF; DPSS; Slepian basis; waveform concentration; operator theory



Citation: Baddour, N.; Sun, Z. Evaluation of the Prolate Spheroidal Wavefunctions via a Discrete-Time Fourier Transform Based Approach. *Symmetry* **2023**, *15*, 2191. <https://doi.org/10.3390/sym15122191>

Academic Editor: Manuel Gadella

Received: 1 September 2023

Revised: 29 November 2023

Accepted: 1 December 2023

Published: 12 December 2023



Copyright: © 2023 by the authors. Licensee MDPI, Basel, Switzerland. This article is an open access article distributed under the terms and conditions of the Creative Commons Attribution (CC BY) license (<https://creativecommons.org/licenses/by/4.0/>).

1. Introduction

To what extent can a bandlimited function be concentrated in the time domain? This question has been investigated by several researchers and most famously addressed in a series of seminal papers by Slepian, Landau and Pollock [1–5]. This resulted in a new class of bandlimited functions with a distinctive combination of characteristics, which were identified as prolate spheroidal wave functions (PSWFs) because of a ‘lucky accident’ of Slepian et al. In addition to certain orthogonality properties, the most valuable characteristic of the PSWFs is their property of optimal energy concentration. PSWFs form an orthogonal basis set over a finite interval, as well as being orthogonal over infinity. Another important property is that their Fourier transform is a scaled version of itself. Such desirable physical and mathematical properties led to many applications that use PSWFs in such diverse domains. For example, in radio astronomical source modelling [6], PSWFs can model the source with a minimum number of basis functions and fewer artifacts outside the region of interest (ROI). On the assessment of ship responses [7,8], PSWFs can be used not only to represent

ocean waves, but also to smooth the measured autocorrelation function and associated power spectrum densities. In the application of beam forming in 1D and 2D [9], using first order PSWFs as a filter window can achieve near optimal performance but with less computational cost. Magnetic resonance imaging (MRI) [10] applies a matching 2D-PSWF filter so that optimal signal concentration and minimal truncation artifacts are achieved. Other applications, such as noise filtering for chipless RFID [11], improving the spectral utilization of communication systems [12], MIMO radar [13], satellite navigation [14], and diffuse sound pressure fields [15] also make use of PSWFs.

Discrete prolate spheroidal sequences (DPSSs) are a set of sequences (vectors) that have somewhat similar energy-concentration properties as PSWFs. DPSSs are orthogonal bandlimited sequences that are most concentrated to a given index range in the time domain. They are often referred to as a “discrete version of PSWFs”. This is correct, in the sense that the DPSSs solve a bandlimited, index-concentrated version of the energy-concentration problem. The DPSSs are discrete sets of vectors and are not usually directly associated with the PSWF (continuous functions) themselves.

The numerical calculation of the PSWFs is a non-trivial problem. The PSWFs can be defined from either an integral equation or a differential equation formulation [1,16]. Hence, their calculation can also be approached from finding numerical solutions to either. Many authors have considered these numerical computations, from both the integral and differential equation definitions. Boyd provided the algorithms and MATLAB codes for computing the PSWFs and their eigenvalues using a Legendre–Galerkin discretization of the prolate differential equation [17]. The PSWFs were then found from a Legendre series with coefficients provided by eigenvectors of the matrix eigenproblem. Schmutzhard et al. [18] also investigated the truncation of the infinite eigensystem where the Legendre–Galerkin method was used to compute the PSWFs from their differential operator definition. Osipov and Rokhlin considered quadrature rules for the integration of the PSWFs [19]. Their work follows on other works that considered quadrature and interpolation, for example, Xiao et al. [20]. Xiao et al. based their work on an infinite series of Legendre polynomials, considering the integral equation formulation of the problem. They based their Legendre polynomial approach on the classical method of Bouwkamp, who considered the differential equation definition [21]. Karoui and Moumni used normalized Legendre polynomials to discretize the definition of the PSWFs as eigenfunctions of the finite-Fourier transform and returned the values at the Shannon sampling points [22]. In a further work, Bonami and Karoui used the Legendre complete elliptic integral of the first kind to provide explicit approximations of the function and their eigenvalues [23]. Many other works have considered the numerical computation of the PSWFs, both from the integral or differential equation approach [24–34].

A marked shift from approaching the numerical computation of the PSWFs from the quadrature or special function approaches considered above involved using the Shannon sampling theorem. Khare and George introduced an approach to computing the PSWFs using a sampling theory approach [35]. Walter and Soleski also proposed a very similar approach, again using the sampling theorem [36–38]. The method in this approach leads to an eigenvalue problem for an (infinite) matrix operator equivalent to that of the integral operator. Truncation of the infinite matrix leads to a finite dimensional matrix eigenvalue/eigenvector problem. Their computationally friendly approach gives the values of the PSWFs on the real line, at the Shannon sampling points. Interpolation with sinc functions is then required to obtain sampled values of the PSWF at points other than the Shannon sampling points. Hogan and Lakey extended the work of Walter and Shen to establish error estimates of the eigenfunction samples and on the matrices used to generate these sample approximations [39].

Linear operators have been studied in the context of many applications of mathematics from the past to the present [40–42]. In this paper, we approach the problem of computation of the PSWF from the point of view of applying operator theory to the discrete Fourier transform (DFT) and solving the PSWF in discrete time. This leads to an infinite dimensional

matrix operator eigenvalue problem, which we recognize as being the definition of the DPSSs. The truncation of the infinite matrix introduces some error but leads to a finite dimensional matrix eigenvalue problem which in turn yields what is known as the Slepian basis. These discrete-valued Slepian basis vectors can then be used (with some error) as discrete time evaluations of the PSWF—in other words, direct approximations to sampled values of the PSWF. The main merits of using the Slepian basis as discrete time evaluation of PSWF is to avoid the computation of the integral or differential operator, as in [19–21], and because it does not require reconstruction, as in the Shannon sampling approach [35]. Although this approach has some errors especially when the number of points is small, the reconstruction algorithm using sinc series is provided in Section 5.4 to retain detail in between the sample points.

The outline of this paper is as follows. Section 2 introduces the PSWFs. Section 3 introduces the time and band-limiting operators in continuous time and frequency. Section 4 formulates the concentration problems in terms of operators. Section 5 implements the operator approach to discrete time—this is the theoretical core of the present paper. Section 6 compares this approach with the classic Shannon sampling approach. In Section 7, the proposed approach for calculating the PSWFs is implemented, analyzed, and discussed. Section 8 summarizes and concludes the paper.

2. Introduction to PSWFs

In this section, we introduce the definitions of the PSWFs. The PSWFs arise in various science- and engineering-related applications. They can be considered as eigenfunctions of either a differential operator or a (non-obviously) related integral operator, corresponding to two distinct classes of physical phenomena. In this paper, we are interested in the time–frequency–concentration properties of PSWFs and present them as solutions to time–frequency–concentration problems. We begin our definitions by introducing the energy–concentration problems that led Slepian to discover the connection between energy–concentration and PSWFs [1].

2.1. Energy Concentration Ratios

We start by defining the energy-concentration ratios. For a given finite bandwidth $[-W, W]$ (W in rad/s) and duration $[-T, T]$ (T in seconds), we define the energy-concentration ratios for a signal $f(t)$ and its Fourier transform $F(\omega)$ in time and angular frequency domains as

$$\alpha = \frac{\int_{-T}^T |f(t)|^2 dt}{\int_{-\infty}^{\infty} |f(t)|^2 dt} \quad (1)$$

and

$$\beta = \frac{\int_{-W}^W |F(\omega)|^2 d\omega}{\int_{-\infty}^{\infty} |F(\omega)|^2 d\omega} \quad (2)$$

Hence, α represents the fraction of the total energy of the signal concentrated in the time interval $|t| \leq T$ and β represents the fraction of the total energy of the signal concentrated in the frequency bandwidth with width $|\omega| \leq W$.

2.2. Problem Statement

Some of the questions that Slepian, Pollak, and Landau set out to answer in [1,6] were:

1. **Time-concentration problem:** if a function $f(t)$ is bandlimited (or equivalently $\beta = 1$ and W is finite), what range of time-concentration ratios α is achievable and what type of function can achieve the maximum concentration?

2. **Frequency-concentration problem:** if a function $f(t)$ is timelimited (or equivalently $\alpha = 1$ and T is finite), what range of frequency-concentration ratios β is achievable and what type of function can achieve the maximum concentration?

2.3. Solution to the Time-Concentration Problem

It can be shown that the solution to the time-concentration problem (Problem 1) can be solved in either the time domain or frequency domain [1,16,43]. The solution is provided by the functions that satisfy the following integral eigenequation in the frequency domain,

$$\int_{-W}^W F(p) \frac{\sin(T(\omega - p))}{\pi(\omega - p)} dp = \lambda F(\omega) \quad |\omega| \leq W \quad (3)$$

Here, λ are the eigenvalues of the eigenequation and achieve the stationary points of the ratio in Equation (1). W and T are defined independently, where W is the band limit of the eigenfunction and $[-T, T]$ is the time concentration interval (solution to Problem 1). Equivalently, the solution is provided by the functions that satisfy the following integral eigenequation in the time domain,

$$\int_{-T}^T f(p) \frac{\sin(W(t - p))}{\pi(t - p)} dp = \lambda f(t) \quad -\infty < t < \infty \quad (4)$$

The solutions to Equation (3) or equivalently (4) are a set of functions known as the prolate spheroidal wave functions (PSWFs) and have many important properties that have been listed elsewhere [1,16,43]. The PSWFs and their corresponding eigenvalues form an infinitely countable, orthogonal set of bandlimited eigenfunctions of Equation (3) or (4). Countable means that the set can be put in one-to-one correspondence with the set of natural numbers. This set is the set of bandlimited, time-concentrated PSWFs, bandlimited to $[-W, W]$ and time-concentrated in $[-T, T]$.

2.4. Solution to the Frequency-Concentration Problem

Similar to the above, it can be shown that the solution to the frequency-concentration problem (Problem 2) can be solved in either the time or the frequency domain [1,16,43]. The solutions are provided by the functions that satisfy the following integral eigenequation in the time domain,

$$\int_{-T}^T f(s) \frac{\sin(W(t - s))}{\pi(t - s)} ds = \lambda f(t) \quad |t| \leq T \quad (5)$$

Here, λ are the eigenvalues of the eigenequation and achieve the stationary points of the ratio in Equation (2). Equivalently, the solutions are given by the functions that satisfy the following integral eigenequation in the frequency domain,

$$\int_{-W}^W F(s) \frac{\sin(T(\omega - s))}{\pi(\omega - s)} ds = \lambda F(\omega) \quad -\infty < \omega < \infty \quad (6)$$

The solutions to Equations (5) or (6) are also prolate spheroidal wave functions (PSWFs). These PSWFs and their corresponding eigenvalue form an infinitely countable, orthogonal set of timelimited eigenfunctions of Equations (5) or (6). These are the timelimited, frequency-concentrated PSWFs, timelimited in $[-T, T]$ and frequency-concentrated in $[-W, W]$.

2.5. Comparison of the Time and Frequency Concentration Problems

Consider a side-by-side comparison of Equations (3) and (5):

$$\begin{aligned} \text{Problem 1} \quad & \int_{-W}^W F(p) \frac{\sin(T(\omega-p))}{\pi(\omega-p)} dp = \lambda F(\omega) \quad |\omega| \leq W \\ \text{Problem 2} \quad & \int_{-T}^T f(s) \frac{\sin(W(t-s))}{\pi(t-s)} ds = \lambda f(t) \quad |t| \leq T \end{aligned} \quad (7)$$

There is a clear time/frequency symmetry between Equations (3) and (5). Furthermore, they are identical, apart from interchanging the role of time and frequency. In other words, the equations are identical if $f(t)$ is replaced with $F(\omega)$, time t is replaced with angular frequency ω , T is replaced with W and W is replaced with T . That is, the role of time and frequency are completely interchanged. The eigenvalues for the W bandlimited, T time-concentrated PSWFs are the same as the eigenvalues of the T timelimited, W band-concentrated PWSFs.

We can also see this connection in another way by introducing two simple changes in the variable, provided via

$$\frac{\omega T}{W} = t \quad \text{and} \quad \frac{p T}{W} = s \quad (8)$$

These changes in variables demonstrate that if $\Psi_n(\omega)$ is an eigensolution to (3), then $\Psi_n(\omega T/W)$ is an eigensolution to (5) [43]. In other words, the frequency-concentration problem is the symmetric dual of the time-concentration problem—which explains the above comments that a set of PSWFs are eigenfunctions of either the frequency- or time-concentration problems. Hence, we only need to solve one set of eigenequations since the mathematical structure of both problems is the same, albeit with a change in variables to switch from one problem to the other.

Another insight can be gained through comparing Problems 1 and 2 by comparing Equation (4) with Equation (5), now both equations in the same domain. These are reproduced here for convenience:

$$\begin{aligned} \text{Problem 1} \quad & \int_{-T}^T f(p) \frac{\sin(W(t-p))}{\pi(t-p)} dp = \lambda f(t) \quad -\infty < t < \infty \\ \text{Problem 2} \quad & \int_{-T}^T f(s) \frac{\sin(W(t-s))}{\pi(t-s)} ds = \lambda f(t) \quad |t| \leq T \end{aligned} \quad (9)$$

It is noted from the preceding side-by-side comparison that time-limiting the result of Problem 1 to $[-T, T]$ yields Problem 2.

It is important to remark that some other authors use the $[-T/2, T/2]$ time concentration interval rather than $[-T, T]$ as proposed here. The advantage of the $[-T, T]$ time interval is that there is complete symmetry between time and frequency domains; variables can be interchanged without having to account for a factor of 2.

3. Band-Limiting and Time-Limiting Operators

It is useful to consider the problems above from the point of view of operator theory. This allows powerful results from functional analysis to be used and also allow us to make the connection from the PSWF set of functions to the DPSS set of vectors. To proceed in this fashion, we introduce the band-limiting and time-limiting operators in both frequency and time domains. This operator theory approach allows us to demonstrate how the DPSS can be used to evaluate the PSWF at discrete points.

3.1. Band-Limiting Operator Action

Let B_σ be the (self-adjoint and idempotent) projection operator action of projecting into the subspace \mathbb{F}_σ of bandlimited functions with the maximum angular frequency σ . The units of σ are radians per second and we will make use of $\sigma = 2\pi B$ if the desired maximum frequency, B , needs to be specified in Hertz. That is, multiplication or division by 2π , as appropriate, ensures that the final values are given in the desired units. The band limiting operator action B_σ for $\sigma > 0$ takes a function as input and returns a frequency-limited version of the function as output where the frequencies are limited to $[-\sigma, \sigma]$. It is defined in frequency space as

$$\tilde{B}_\sigma[F](\omega) = \begin{cases} F(\omega) & \text{if } |\omega| \leq \sigma \\ 0 & \text{if } |\omega| > \sigma \end{cases} \tag{10}$$

The tilde (\sim) over the operator action is used to denote that the operator action is taking place in the frequency domain. In the time domain, the operator action is provided by:

$$B_\sigma[f](t) = \frac{1}{2\pi} \int_{-\sigma}^{\sigma} F(\omega) e^{i\omega t} d\omega \quad -\infty < t < \infty \tag{11}$$

In Equation (11), $F(\omega)$ is the Fourier transform of $f(t)$ and the band-limiting operator action is denoted without the tilde since it is taking place in the time domain. The form of the operator in Equation (11) is not that useful since it acts on $f(t)$, on the left-hand side, but $F(\omega)$ appears on the right-hand side. We need to rewrite the operator so that it acts directly on $f(t)$. Using the definition of the Fourier transform (see Appendix A and [44]), then:

$$\begin{aligned} B_\sigma[f](t) &= \frac{1}{2\pi} \int_{-\sigma}^{\sigma} F(\omega) e^{i\omega t} d\omega \\ &= \frac{1}{2\pi} \int_{-\sigma}^{\sigma} \int_{-\infty}^{\infty} f(s) e^{-i\omega s} ds e^{i\omega t} d\omega \\ &= \int_{-\infty}^{\infty} \frac{1}{2\pi} \int_{-\sigma}^{\sigma} e^{-i\omega s} e^{i\omega t} d\omega f(s) ds \end{aligned} \tag{12}$$

This becomes

$$B_\sigma[f](t) = \int_{-\infty}^{\infty} K_\sigma(t, s) f(s) ds \quad t \in \mathbb{R} \tag{13}$$

where the operator kernel is provided by

$$K_\sigma(t, s) = \frac{1}{2\pi} \int_{-\sigma}^{\sigma} e^{-i\omega s} e^{i\omega t} d\omega = \frac{\sin(\sigma(s - t))}{\pi(s - t)} \tag{14}$$

The form of the operator in Equations (13) and (14) is the desired form, since now the definition of the operator acts on $f(t)$ (the same function) on both sides of the equation. The self-adjointness of B_σ is easily established since the kernel $K_\sigma(t, s)$ is real and symmetric, i.e., $K_\sigma(t, s) = K_\sigma(s, t)$ [43], as can be seen from its integral definition in Equations (13) and (14).

Hence, $B_\sigma[f]$ and $\tilde{B}_\sigma[F]$ form a Fourier pair, $B_\sigma[f] \Leftrightarrow \tilde{B}_\sigma[F]$, which means applying the operator B_σ on f in the time domain is equivalent to applying the operator \tilde{B}_σ on F (the Fourier transform of f) in the frequency domain. The frequency-limiting operator can be applied in either domain, by implementing its appropriate mathematical form in each domain.

3.2. Time-Limiting Operator Action

Similarly, let B_T be the (self-adjoint and idempotent) projection operator action of projecting into the subspace \mathbb{F}_T of time-limited functions limited to the time interval $|t| \leq T$. Then, the time-limiting operator action B_T is defined in the time domain as

$$B_T[f](t) = \begin{cases} f(t) & \text{if } |t| \leq T \\ 0 & \text{if } |t| > T \end{cases} \quad (15)$$

In the frequency domain, the operator action is given by:

$$\tilde{B}_T[F](\omega) = \int_{-T}^T f(t)e^{-i\omega t} dt \quad -\infty < \omega < \infty \quad (16)$$

Once again, the tilde over the operator action is used to denote that the operator is acting in the frequency domain. As above, we want to recast Equation (16) so that it operates on the same form of the function on both sides of the equation. Following the methodology of above and using the definition of the Fourier transform, then

$$\tilde{B}_T[F](\omega) = \int_{-\infty}^{\infty} K_T(\omega, s)F(s)ds \quad (17)$$

where the operator kernel is given by

$$K_T(\omega, s) = \frac{1}{2\pi} \int_{-T}^T e^{ist} e^{-i\omega t} dt = \frac{\sin(T(s - \omega))}{\pi(s - \omega)} \quad (18)$$

Equation (17) is the requisite form as it applies to the same form of the function on both sides of the equation. As above, the self-adjointness of \tilde{B}_T is established since it is real and symmetric, which is clear from its integral definition in Equations (17) and (18). As above, $B_T[f]$ and $\tilde{B}_T[F]$ form a Fourier pair, $B_T[f] \Leftrightarrow \tilde{B}_T[F]$. That is, applying the operator B_T on f in the time domain is equivalent to applying the operator \tilde{B}_T on F (the Fourier transform of f) in the frequency domain. The time-limiting operator can be applied in either domain, by implementing its appropriate mathematical form in each domain.

4. Concentration Problems in Terms of Operators

As noted above, the time-concentration and frequency-concentration problems are essentially the same problem, with the roles of time and frequency (and the appropriate variables T and W) interchanged. Hence, it suffices to focus on only one problem. We return to the definition of the time-concentration problem, which is: if a function is bandlimited (or equivalently $\beta = 1$), what range of time-concentration ratios α is achievable and what type of function can achieve the maximum concentration?

We rewrote the problem in terms of the time- and band-limiting operators. Using the idempotent and self-adjoint properties of the operator, we can make use of the inner product notation for energy and write the time-concentration ratio in the time domain as

$$\alpha = \frac{\int_{-T}^T |B_W f(t)|^2 dt}{\int_{-\infty}^{\infty} |B_W f(t)|^2 dt} = \frac{\langle B_T B_W f, B_T B_W f \rangle}{\langle B_W f, B_W f \rangle} = \frac{\langle B_W B_T B_T B_W f, f \rangle}{\langle B_W B_W f, f \rangle} = \frac{\langle B_W B_T B_W f, f \rangle}{\langle B_W f, f \rangle} \quad (19)$$

Here, we use the L^2 Hermitian inner product between two functions on a measure space with measure μ given by

$$\langle f, g \rangle = \int_{-\infty}^{\infty} f \bar{g} d\mu \quad (20)$$

In Equation (19), we first used the self-adjoint property to transfer the operators to the left-hand side of the inner product operator and then used the idempotent property of each to obtain the final equality.

Using Parseval's relation, Equation (19) can also be written in the frequency domain as

$$\alpha = \frac{\langle B_W B_T B_W f, f \rangle}{\langle B_W f, f \rangle} = \frac{\langle \tilde{B}_W \tilde{B}_T \tilde{B}_W F, F \rangle}{\langle \tilde{B}_W F, F \rangle} \quad (21)$$

4.1. Operator Interpretation of the Time Concentration Problem-Time Domain

In the time domain, Equation (19) can be rearranged as

$$\langle B_W B_T B_W f, f \rangle = \alpha \langle B_W f, f \rangle \quad (22)$$

The concentration ratio is maximized when f satisfies the eigenvalue problem given by

$$B_W B_T B_W f = \lambda B_W f \quad \text{or} \quad B_W B_T g = \lambda g \quad (23)$$

where $g = B_W f$. Hence, the maximum value of the time-concentration ratio, α , is achieved for the largest eigenvalue λ in Equation (23).

Applying the definition of the operator B_W given in Equation (13) and the definition of operator B_T given in Equation (15) to $B_W B_T g = \lambda g$ in Equation (23) yields exactly the eigenequation given in Equation (4). Hence, we obtain

$$B_W B_T g = \int_{-T}^T g(p) \frac{\sin(W(t-p))}{\pi(t-p)} dp = \lambda g(t) \quad -\infty < t < \infty \quad (24)$$

Thus, the W bandlimited, T time-concentrated PSWFs are an infinitely countable set of bandlimited functions, denoted by $\phi^n(t)$, with a corresponding eigenvalue λ_n that satisfies (24) or equivalently $B_W B_T \phi^n = \lambda_n \phi^n$. That is, the W bandlimited, T time-concentrated PSWFs are eigenfunctions of the time-limiting, followed by the band-limiting operator. We use the superscript notation to count the eigenfunctions since the subscript notation will be used to denote discretization later in this paper.

4.2. Operator Interpretation of the Time-Concentration Problem-Frequency Domain

In the frequency domain, Equation (21) can be rearranged as

$$\langle \tilde{B}_W \tilde{B}_T \tilde{B}_W F, F \rangle = \alpha \langle \tilde{B}_W F, F \rangle \quad (25)$$

As above, the maximum concentration ratio is given by solving the eigenvalue problem

$$\tilde{B}_W \tilde{B}_T \tilde{B}_W F = \lambda \tilde{B}_W F \quad (26)$$

Applying the definitions of \tilde{B}_W and \tilde{B}_T given in Equations (10) and (17) to $\tilde{B}_W \tilde{B}_T \tilde{B}_W F = \lambda \tilde{B}_W F$ yields exactly the eigenequation given in Equation (3), represented by:

$$\int_{-W}^W F(p) \frac{\sin(T(\omega-p))}{\pi(\omega-p)} dp = \lambda F(\omega) \quad |\omega| \leq W \quad (27)$$

Thus, solving $\tilde{B}_W \tilde{B}_T \tilde{B}_W F = \lambda \tilde{B}_W F$ in the frequency domain also yields the W bandlimited, T time-concentrated PSWFs, but now in the frequency domain. That is, the PSWFs are an infinitely countable set of eigenfunctions that satisfy $\tilde{B}_W \tilde{B}_T \tilde{B}_W \Phi^n = \lambda_n \tilde{B}_W \Phi^n$, where Φ^n are the Fourier transforms of ϕ^n .

4.3. Operator Interpretation of the Frequency-Concentration Problem

We can follow the same steps as above to interpret the frequency-concentration problem (Problem 2) in the time and frequency domains. Following the methodology for the time-concentration problem, it can be shown that the frequency-concentration problem can be written as an eigenfunction problem that needs to satisfy $B_T B_W B_T f = \lambda B_T f$ in the time domain and $\tilde{B}_T \tilde{B}_W G = \lambda G$ (where $G = \tilde{B}_T F$) in the frequency domain. Applying the definitions of the time- and band-limiting operators in the appropriate domains yields the eigenequations provided in Equations (5) and (6).

We stated in the previous section that the W bandlimited, T time-concentrated PSWFs $\phi^n(t)$ satisfy $B_W B_T \phi^n = \lambda_n \phi^n$ in the time domain. Adding one more time-limiting operator to both sides yields:

$$B_T B_W B_T \phi^n = \lambda_n B_T \phi^n \quad (28)$$

In other words, $B_T \phi^n$ solves Equation (5), which is the eigenproblem that defines the frequency-concentration problem (Problem 2) yielding the T timelimited and W band-concentrated PSWFs. The eigenvalues are the same as for the time-concentration problem.

5. Discrete Time Fourier Transform Interpretation of the Operators

In the previous section, we demonstrated how the PSWFs can be found from an operator theoretical point of view using time- and band-limiting operators in sequence. In this section, we apply a discrete-time approach to the evaluation of the PSWFs. We will demonstrate how implementation of the operators using the discrete time Fourier transform (DTFT), leads to discrete prolate spheroidal sequence (DPSS) [5] and Slepian-based approximations of the PSWFs. The key to establishing the connection between the PSWF and DPSS is the use of the DTFT. The DTFT is a transform that operates on discrete time data to give a continuous function of frequency. It can be considered as a transform that connects the discrete time domain to the continuous frequency domain (forward transform and inverse transform). Although it connects any form of discrete data (which is the interpretation given in [5]), in this work we interpret the discrete data to be samples of a continuous function, which allows us to connect the continuous PSWFs to the DPSSs that arise as a result of the eigenfunction problem.

5.1. Discrete-Time Interpretations of the Eigenequation of Problem 1

We showed in the previous section that the PSWFs are defined from the eigenequation $B_W B_T g = \lambda g$ in the time domain. In the following section, we apply the above operators to a discrete-time function, that is, we consider g in discrete time. To implement the band- and time-limiting operators in discrete time, we refer to the DTFT. That is, we need to interpret the operators using the appropriate definition of the Fourier transform for functions in discrete time.

We start with the definition of the DTFT, a Fourier transform that operates on discrete time data. We are interested in domains of $[-T, T]$ in the time domain, and $[-W, W]$ in the frequency domain. Here, W is in units of radians per second, so the equivalent domain in Hertz is $[-B, B]$ where $W = 2\pi B$. We will discretize our problem to a dimension of N where N is an integer.

Suppose we start with a discrete-time function given by $f_n = f\left(\frac{n}{F_s}\right)$, where F_s is the sampling frequency and n is a counter variable. The evaluations $f\left(\frac{n}{F_s}\right)$ are samples of $f(t)$ defined at specific instances on the real line. We choose the sampling frequency given by $F_s = \frac{1}{\Delta t} = \frac{N-1}{2T}$ Hz (or $2\pi F_s$ rad/s), where the sampling interval has been chosen as $\Delta t = \frac{2T}{N-1}$ and N is the chosen dimension of the problem. The $N - 1$ factor arises so

that there will be exactly N points in the interval $[-T, T]$, including both endpoints of the interval. In other words, given a domain of interest $[-T, T]$, choosing N determines both the sampling rate F_s and the dimension of the system N that we will be considering.

Then, the definition of the DTFT provides the relationship between the discrete samples $f\left(\frac{n}{F_s}\right)$ and its continuous Fourier transform $F(\omega)$ as

$$F(\omega) = \sum_{n=-\infty}^{\infty} \frac{1}{F_s} f\left(\frac{n}{F_s}\right) e^{-i\frac{n}{F_s}\omega} \quad (29)$$

The inverse transform returns the original discrete time function from

$$f\left(\frac{n}{F_s}\right) = \frac{1}{2\pi} \int_{-\pi F_s}^{+\pi F_s} F(\omega) e^{i\frac{n}{F_s}\omega} d\omega \quad -\infty < n < \infty \quad (30)$$

Note that the limits of integration in Equation (30) are from $[-\pi F_s, \pi F_s]$ rad/s or $\left[-\frac{F_s}{2}, \frac{F_s}{2}\right]$ Hz. In other words, the effect of sampling the function at a frequency of F_s Hz is equivalent to band-limiting the function between $\left[-\frac{F_s}{2}, \frac{F_s}{2}\right]$ Hz. Alternatively, if the function is known to be bandlimited with a max frequency $F_s/2$, then sampling the function at F_s guarantees that we can perfectly calculate its DTFT and reconstruct the function; there is no loss of information.

Given the space of discrete-time functions $f_n = f\left(\frac{n}{F_s}\right)$ and the corresponding appropriate Fourier transform (DTFT), we want to implement the operator eigenequation $B_W B_T f_n = \lambda f_n$ on this space. To do so, we need forms of the operators B_W and B_T that are appropriate for the space.

We want to consider how to implement the time-limiting operator, B_T , that is to limit a function between $[-T, T]$. Given our choice of discretization, this is equivalent to limiting the counter n to be between $n \in \left[-\frac{(N-1)}{2}, \frac{N-1}{2}\right]$. Hence, this implies

$$B_T f_n = B_{\frac{N-1}{2}} f_n = \begin{cases} f_n & -\frac{N-1}{2} \leq n \leq \frac{N-1}{2} \\ 0 & \text{otherwise} \end{cases} \quad (31)$$

Next, we need to implement a band-limiting operator in the discrete-time domain of the DTFT. Previously in this paper, we implemented the band-limiting operator in the continuous time domain; however, here, we need to interpret it for the discrete-time domain. To implement a band-limiting operator to frequency range $[-W, W]$, then we use Equation (30) with the given bandlimit, so that:

$$B_W f_n = B_W f\left(\frac{n}{F_s}\right) = \frac{1}{2\pi} \int_{-W}^W F(\omega) e^{i\frac{n}{F_s}\omega} d\omega \quad (32)$$

In Equation (32), it is imperative that the band-limit is 'tighter' than the given information in the problem. That is, Equation (32) only makes sense if $W < \pi F_s$ in radians or equivalently $B < F_s/2$ ($W = 2\pi B$) since there is no information about the function past frequency $F_s/2$.

Equation (32) can be put in the proper discrete-time form (that is, as an operator acting on f_n rather than $F(\omega)$) by substituting the definition of $F(\omega)$ from Equation (29) into Equation (32). This gives

$$B_W f_n = B_W f\left(\frac{n}{F_s}\right) = \frac{1}{2\pi} \int_{-W}^W \left\{ \sum_{m=-\infty}^{\infty} \frac{1}{F_s} f_m e^{-i\frac{m}{F_s}\omega} \right\} e^{i\frac{n}{F_s}\omega} d\omega \quad (33)$$

Interchanging the order of summation and integration in Equation (33) gives

$$B_W f_n = \sum_{m=-\infty}^{\infty} f_m \frac{\sin\left(\frac{2TW(m-n)}{N-1}\right)}{\pi(m-n)} \quad -\infty < m, n < \infty \quad (34)$$

Now, we put all our definitions and implementations of operators to define the desired eigenequation in discrete time. Our desired equation is $B_W B_{\frac{N-1}{2}} f_n = \lambda f_n$. Using Equations (31) and (34), this yields the eigenequation implemented in discrete time as

$$\sum_{m=-\frac{(N-1)}{2}}^{\frac{N-1}{2}} f\left(\frac{m}{F_s}\right) \frac{\sin\left(\frac{2TW(m-n)}{N-1}\right)}{\pi(m-n)} = \lambda f\left(\frac{n}{F_s}\right) \quad -\infty < n < \infty \quad (35)$$

Equation (35) implements the PSWF-defining operator eigenequation in discrete time. That is, it implements the discrete time equivalent of the same set of operators that return the PSWF in continuous time. Hence, the discrete time eigenvectors returned by (35) should return (approximations to) sampled values of the W -bandlimited, T -time concentrated continuous PSWFs. Furthermore, the eigenvalues should also be (approximations to) the eigenvalues for the time-concentration problem (Problem 1). Although we are applying the discrete-time equivalent of the operators that define the original PSWF, the action of the operators in their respective domains introduces some differences. There is some error introduced in going from $B_W B_T f = \lambda f$ to $B_W B_{\frac{N-1}{2}} f_n = \lambda f_n$ since after time-limiting, the function loses its bandlimitedness (prior to the application of the band-limiting operator) which means that the DTFT representation now has some error. We will examine the practical implications of this through simulations in the next section.

The kernel of the transformation in Equation (35) is the (infinite) matrix representation of the operator $B_W B_T = B_W B_{\frac{N-1}{2}}$. It can be written for $m \in \left[-\frac{(N-1)}{2}, \frac{N-1}{2}\right]$ and $n \in [-\infty, \infty]$ as

$$\frac{\sin\left(\frac{2TW(m-n)}{N-1}\right)}{\pi(m-n)} = \frac{\sin\left(\frac{2\pi \cdot 2TB(m-n)}{N-1}\right)}{\pi(m-n)} = \frac{\sin\left(2\pi\left(\frac{B}{F_s}\right)(m-n)\right)}{\pi(m-n)} \quad (36)$$

Since $B < F_s/2$, as described above, it then follows that $B/F_s < 1/2$. In the case of the hard inequality $B/F_s < 1/2$, Equation (35) is also the defining equation for the discrete prolate spheroidal sequences (DPSSs). The defining equations for the DPSSs traditionally use $\frac{\sin(2\pi\sigma(m-n))}{\pi(m-n)}$ in the kernel, where $\sigma < 1/2$. Hence, converting from our notation to traditional DPSS definition, we have $\sigma = B/F_s$, thereby demonstrating the connection between the traditional DPSSs and the (approximate) sampled values of the PSWFs.

The requirement $B/F_s < 1/2$ is equivalent to the classical Shannon sampling theorem statement that $2B < F_s$. Shannon allowed equality to hold, that is, the minimum sampling rate is $F_s = 2B$. The statement $2B < F_s$ can also be rewritten in terms of the definition of F_s as

$$2B < \frac{N-1}{2T} \quad \Rightarrow \quad 4BT + 1 < N \quad (37)$$

The selection of N controls the sampling of the function and the sampling rate F_s . A larger N implies more detail and a finer sampling of the interval $[-T, T]$. The smallest allowable value of N must satisfy Equation (37), which is the equivalent of the statement of the Shannon sampling theorem.

We note from Equation (36) that the parameters T and B (or equivalently W) are the ones used to define the continuous time PSWFs. However, N is the parameter chosen to represent the discrete time version of the problem by controlling the sampling rate F_s . Choosing different values of N will return a different DPSS, that is a different DPSS (controlled by T , B and N) that can be used to approximate the PSWF (controlled by T and

B). The ‘approximation’ of the PSWF by the DPSS is controlled by the choice of N . The choice of N allows us to start with f_n , a discrete time function, before applying the operator eigenequation $B_W B_T f_n = \lambda f_n$. The operator equation $B_W B_T f_n = \lambda f_n$ is equivalent to applying the continuous operators $B_W B_T B_{F_s/2} f = \lambda B_{F_s/2} f$ since discretization can be considered equivalent to applying a band-limiting operator. In contrast, the true PSWF itself is the result of applying the operator eigenequation $B_W B_T f = \lambda f$ to a continuous time function.

5.2. Time-Bandwidth Product and the Shannon Number

The product $c = 2BT = \frac{WT}{\pi}$ (where $W = 2\pi B$) is called the time-bandwidth product of the PSWFs and represents the degrees of freedom of the function [45]. This represents the minimum number of samples of a signal required to represent it in a fairly accurate manner [35]. In much of the literature on PSWFs, the parameter $2\pi BT = WT$ is referred to as the Shannon number and is related to the time-bandwidth product [45]. Some care needs to be taken in comparing various works as some authors use $[-T/2, T/2]$ as the time interval instead of $[-T, T]$. Most of the literature on PSWFs studies their properties based on the definition as a solution of the differential equation depending on the value of c . To further highlight the inconsistencies in terminology, MATLAB refers to $2BT$ as the time (interval duration $2T$), half-bandwidth (B) product. Hence, caution is advised when referring to the ‘time-bandwidth’ product as there are several slightly different definitions that exist in the literature.

5.3. Discrete-Time Interpretation of the Eigenequation of Problem 2

If the transformation kernel of Equation (35) is further restricted to $n \in \left[-\frac{(N-1)}{2}, \frac{N-1}{2}\right]$, then this is the implementation of the operator $B_T B_W B_T = B_{\frac{N-1}{2}} B_W B_{\frac{N-1}{2}}$. The resulting $N \times N$ matrix is known as the prolate matrix and given by:

$$\rho_{m,n} = \frac{\sin\left(2\pi\left(\frac{B}{F_s}\right)(m-n)\right)}{\pi(m-n)} \quad m, n \in [1 \dots N] \quad (38)$$

Note that the summation counter (m) in Equation (35) is for $m \in \left[-\frac{(N-1)}{2}, \frac{N-1}{2}\right]$ while $n \in [-\infty, \infty]$. However, in Equation (38), both counters (m and n) run from 1 to N . Since the kernel/matrix only depends on the difference $m - n$, the statement of Equation (38) with $m, n \in [1 \dots N]$ is correct. The reader is reminded that W in Equation (35) refers to the band-limit in rad/s. The prolate matrix is usually defined in the literature using a normalized frequency between 0 and $1/2$, represented by B/F_s in Equation (38), which is guaranteed to be $< 1/2$ since we imposed the ‘tighter’ bandlimit of $B < F_s/2$.

The matrix in Equation (38) (prolate matrix) is the matrix implementation of the $B_T B_W B_T = B_{\frac{N-1}{2}} B_W B_{\frac{N-1}{2}}$ operator. Hence, the eigenvectors and eigenvalues of that matrix represent an approximation to $B_T B_W B_T f = \lambda f$. For continuous functions f , this is the defining equation for the timelimited band-concentrated PSWFs. Here, we have implemented it on discrete time functions $B_T B_W B_T f_n = \lambda f_n$. Hence, the eigenvectors are, by construction, approximations to the sampled values of the timelimited band-concentrated PSWF, and the eigenvalues are approximations of the eigenvalues for the frequency-concentration problem (Problem 2), as long as f_n is a good representation for f . As discussed above, every application of the time-limiting operator introduces a loss of bandlimitedness and hence some error into a DTFT assumption. Hence, although we have paralleled the defining eigenequation in discrete time, the result cannot be expected to return eigenvalues and eigenvectors that are identical to the continuous time version. There is always some error between the discrete and continuous time versions.

The finite dimensional eigenproblem defined by the prolate matrix in Equation (38) provides a set of finite dimensional eigenfunctions which are known as a Slepian basis.

These are finite-dimensional (truncated) versions of the DPSSs. The DPSS which arise from the eigenvector problem in Equation (35) are of infinite length since $n \in [-\infty, \infty]$.

5.4. Reconstruction from the Discrete Time Values

Since Equation (37) ensures that the Shannon sampling theorem is respected [46], then the continuous time function can be reconstructed after the eigenproblem of Equation (35) is solved. This reconstructs the time-concentrated bandlimited PSWF (band limiting is a requirement of the Shannon sampling theorem). Since the sampling rate F_s may be higher than the minimum required by the Shannon theorem, the interpolation in the time domain is best seen by taking the continuous inverse Fourier transform of Equation (29).

Hence, the DPSS/Slepian approximation to the PSWF is found by first solving the eigenequation implemented in discrete time, given by

$$\sum_{m=-\frac{(N-1)}{2}}^{\frac{N-1}{2}} \phi^p \left(\frac{m}{F_s} \right) \frac{\sin \left(\frac{2TW(m-n)}{N-1} \right)}{\pi(m-n)} = \lambda_p \phi^p \left(\frac{n}{F_s} \right) \quad (39)$$

where ϕ^p is the p th eigenvector corresponding to the p th eigenvalue λ_p . The counter n is infinite $-\infty < n < \infty$ for the DPSS and n is finite for the Slepian bases. The interpolation/reconstruction is performed after the sampled values $\phi_n^p = \phi^p \left(\frac{n}{F_s} \right)$ have been determined from the eigenproblem. From the definition of the inverse Fourier transform and recalling that the resulting function is W -bandlimited (by construction), then the continuous-time PSWFs can be found from

$$\begin{aligned} \Phi^p(\omega) &= \sum_{n=-\infty}^{\infty} \frac{1}{F_s} \phi^p \left(\frac{n}{F_s} \right) e^{-i \frac{n}{F_s} \omega} \\ \frac{1}{2\pi} \int_{-W}^W \Phi^p(\omega) e^{i\omega t} d\omega &= \frac{1}{2\pi} \int_{-W}^W \sum_{n=-\infty}^{\infty} \frac{1}{F_s} \phi^p \left(\frac{n}{F_s} \right) e^{-i \frac{n}{F_s} \omega} e^{i\omega t} d\omega \end{aligned} \quad (40)$$

The left-hand side of Equation (40) is the definition of $\phi^p(t)$. Then, interchanging the summation and integration on the right-hand side gives

$$\phi^p(t) = \sum_{n=-\infty}^{\infty} \phi^p \left(\frac{n}{F_s} \right) \frac{\sin \left(W \left(t - \frac{n}{F_s} \right) \right)}{\pi F_s \left(t - \frac{n}{F_s} \right)} \quad (41)$$

For DPSS solutions, where $-\infty < n < \infty$ then Equation (41) is an infinite sum, as written. For the Slepian bases corresponding to the timelimited, band-concentrated PSWFs, the operation of limiting in time is equivalent to limiting the counter to $n \in \left[-\frac{(N-1)}{2}, \frac{N-1}{2} \right]$. However, it should be noted that once timelimited, a function is no longer bandlimited. This implies that the Shannon sampling theorem with sinc interpolation is no longer exact, which means some error has been introduced.

6. Comparison with Shannon Sampling Approach

Both Khare et al. [35,45] and Walter et al. [36] proposed the computation of the PSWFs using a sinc series along with the Shannon sampling theorem, meaning sampling at precisely $\Delta t = 1/2B$. The sampling theorem allows a bandlimited function $g(x)$ in $L^2(-\infty, \infty)$ with a Fourier transform bandlimited to $[-B, B]$ Hz to be expressed in terms of equally spaced samples that are $\Delta t = 1/2B$ apart. Specifically, it gives the following relations between a bandlimited function $g(x)$ and its samples $g(m/2B)$

$$g(t) = \sum_{m=-\infty}^{\infty} g \left(\frac{m}{2B} \right) \frac{\sin(\pi(2Bt - m))}{\pi(2Bt - m)} \quad (42)$$

Furthermore,

$$g\left(\frac{m}{2B}\right) = 2B \int_{-\infty}^{\infty} g(t) \frac{\sin(\pi(2Bt - m))}{\pi(2Bt - m)} dt \quad (43)$$

Here, we use our operator theory approach as introduced in the first part of this paper, along with Equations (42) and (43) to re-derive the Shannon sampling approach to computing the PSWFs. Specifically, we want to implement the discrete eigenequation $B_B B_T g_n = \lambda g_n$, as above, where now $g_n = g(n/2B)$. That is, g_n are discrete values of the function, with the difference that now we specify the sampling rate to be precisely the Shannon sampling rate.

We want to implement $\lambda g_n = \lambda g\left(\frac{n}{2B}\right) = B_B \{B_T g_n\}$. We consider Equation (43) to be the definition of the band-limiting operator. Hence,

$$B_B \{B_T g\} = 2B \int_{-\infty}^{\infty} \{B_T g(t)\} \frac{\sin(\pi(2Bt - n))}{\pi(2Bt - n)} dt \quad (44)$$

We then use Equation (42) to implement the time-limiting operator as

$$B_T g(t) = \begin{cases} \sum_{m=-\infty}^{\infty} g\left(\frac{m}{2B}\right) \frac{\sin(\pi(2Bt - m))}{\pi(2Bt - m)} & -T \leq t \leq T \\ 0 & \text{otherwise} \end{cases} \quad (45)$$

Inserting Equation (45) into Equation (44) and interchanging the order of integration and summation, then $\lambda g_n = B_B \{B_T g\}$ becomes:

$$\lambda g\left(\frac{n}{2B}\right) = 2B \sum_{m=-\infty}^{\infty} g\left(\frac{m}{2B}\right) \int_{-T}^T \frac{\sin(\pi(2Bt - m))}{\pi(2Bt - m)} \frac{\sin(\pi(2Bt - n))}{\pi(2Bt - n)} dt \quad (46)$$

This can be written as $\lambda g_n = 2B \sum_{m=-\infty}^{\infty} g_m A_{mn}$ where

$$A_{mn} = \int_{-T}^T \frac{\sin(\pi(2Bt - m))}{\pi(2Bt - m)} \frac{\sin(\pi(2Bt - n))}{\pi(2Bt - n)} dt \quad (47)$$

Notably, the infinite matrix defined in Equation (47) is the same as that obtained by Khare [35,45] and Walter [36].

Khare observed that the matrix elements A_{mn} fall off to zero as the main lobes of the corresponding sinc functions go beyond the range of integration, that is when $|m|, |n| > 2TB$. Clearly, only a square sub-matrix of A_{mn} with the dimension of the order of the time-bandwidth product ($4TB$) has elements with significant magnitude [35,45]. Hence, the number of significant eigenvalues is at most of the order of ($4TB$), the remaining eigenvalues being close to zero. The $4TB$ value is the same as that we arrived at in Equation (37).

Solving the eigenvalue problem involves truncating the infinite matrix in Equation (47). For the matrix A_{mn} in (47) to have dimension $N \times N$ implies that the summation in Equation (46) is for $m \in \left[-\frac{N-1}{2} \dots \frac{N-1}{2}\right]$. The sampled values g_n are $1/2B$ apart. The sampled values start at $g\left(-\frac{N-1}{4B}\right)$ and end at $g\left(\frac{N-1}{4B}\right)$. Since the sampled values are $1/2B$ apart, then there are $4TB + 1$ values (the +1 to account for the two endpoints) in the concentration interval $[-T, T]$. Khare observed that the N must be chosen to be 'sufficiently larger' than $4TB + 1$ for this approach to work. Hence, there are $4TB + 1$ data points in the concentration interval, but the information returned extends past the concentration interval itself to $g\left(\pm \frac{N-1}{4B}\right)$. Increasing N implies going out further beyond the endpoints of the concentration interval.

We compare this to our ‘discrete time’ approach taken above where the truncation of the problem also results in an $N \times N$ matrix. However, in our discrete time approach, there are N points inside the concentration interval. Increasing N in this case implies obtaining ‘more detail’ (a finer sampling interval) about the function within the $[-T, T]$ concentration interval. Hence, although both approaches can be truncated into a $N \times N$ matrix eigenvalue problem, the nature of the information returned with the N pieces of information is different. For the Shannon sampling approach, we have information over an interval wider than the concentration interval; for our discrete time approach, we have more information within the concentration interval.

7. Simulations

Section 5 demonstrated that the Slepian basis vectors can be close approximations to the discrete-time values of PSWFs. PSWFs can then be reconstructed from the Slepian basis with Equation (41). In this section, we evaluate numerical simulation results to compare reconstructed Slepian basis values directly with the PSWFs. All simulations were performed using MATLAB. The Slepian bases are obtained through the MATLAB R2019b signal processing toolbox function `dpss`, which calculates the eigenvalues and eigenvectors of the prolate matrix using a fast autocorrelation technique [47]. The errors between eigenvalues found from the Slepian basis approach versus those found directly from the PSWF are calculated via

$$Err = \frac{|\lambda^S - \lambda|}{|\lambda|} \times 100\% \quad (48)$$

where λ is the true eigenvalue from PSWF and λ^S is the eigenvalue obtained from the Slepian basis. The error between two eigenvectors with N points is calculated as a mean error from:

$$Err = \frac{1}{N} \sum_{i=1}^N \frac{|\vec{p}_i - \vec{q}_i|}{\max_i |\vec{q}_i|} \times 100\% \quad (49)$$

where \vec{p}_i and \vec{q}_i are the values of two eigenvectors being compared.

7.1. PSWF Ground Truth

The PSWFs used in the simulations are obtained through the software Chebfun [48], which solves the eigenproblem using the method provided by [20] to compute the normalized Legendre coefficients of the PSWFs by solving an eigenvalue problem. To validate the accuracy of the results of Chebfun, a comparison between the PSWF values obtained through Chebfun and the commonly used Flammer’s tabulated values [49] is provided in Figure 1.

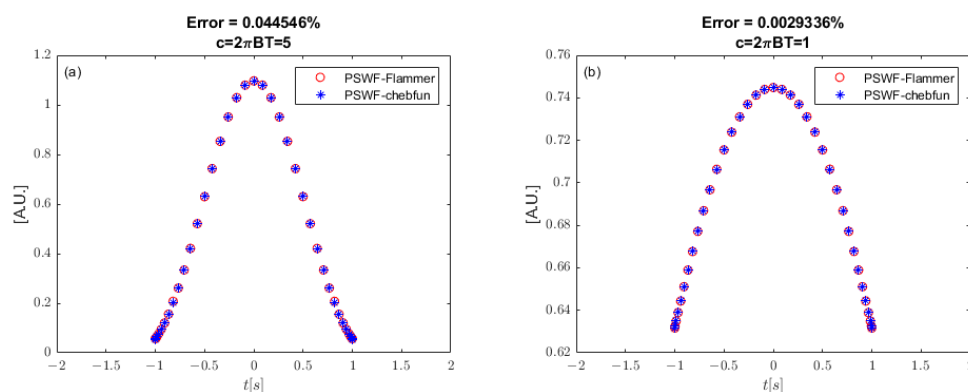


Figure 1. Comparison of PSWFs obtained through the Chebfun software and Flammer’s tabulated values. (a) $c = 5$; (b) $c = 1$.

In Figure 1, PSWFs of order zero for time-bandwidth products $c = 5$ and $c = 1$ are shown. The errors are calculated via Equation (49), where \vec{p}_i represents PSWF values obtained from Chebfun and \vec{q}_i represents PSWF values from Flammer's tabulated values. Results demonstrate accuracy of the Chebfun software for generating PSWF values.

7.2. Slepian Bases and Reconstruction

The Slepian bases are obtained from MATLAB function $[E, V] = DPSS(N, NW)$ written by E. Breitenberger [47], which uses inverse iteration using the exact eigenvalues on a starting vector with approximate shape to obtain the required eigenvectors. It then computes the eigenvalues of the Toeplitz sinc matrix using a fast autocorrelation technique. Here, N is the number of points of Slepian basis and NW is the time-bandwidth product. With the mapping method in [50], the Slepian basis can be mapped to a discrete time vector and consequently, $NW = 2TB$.

Figure 2 shows some examples of Slepian basis ϕ^n with different number of points plotted against time vectors. Here, n is the order of the eigenvector. Note that the Slepian bases are discrete and are approximations of the sampled values of PSWFs.

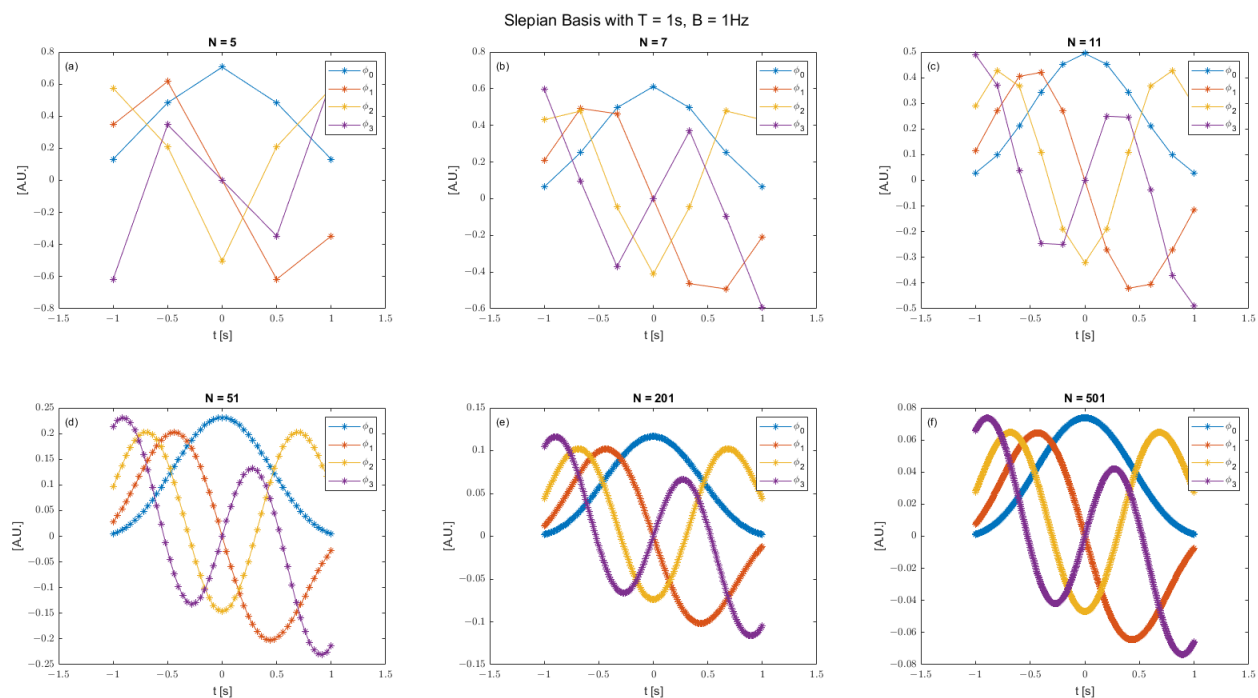


Figure 2. Slepian bases with different number of points N , (a–f) N from 5 to 501.

With the reconstruction method shown in Section 5, we can reconstruct the n th Slepian basis ϕ^n with sinc interpolation to obtain a smooth vector shown in Figure 3. In Figure 3, all vectors are normalized to have unit energy for future convenience in comparison with PSWFs.

7.3. Comparison between Sinc-Series-Reconstructed Slepian Basis and PSWF

In this section, we evaluate the sinc-series-reconstructed Slepian basis with PSWF values obtained through Chebfun. Figures 4–7 show the comparison results for eigenvectors of order 0 to 3. The reconstructed Slepian bases are those shown in Figure 3. As can be seen from the error values in Figures 4–7, as the number of points used to reconstruct the Slepian bases increases, the error decreases.

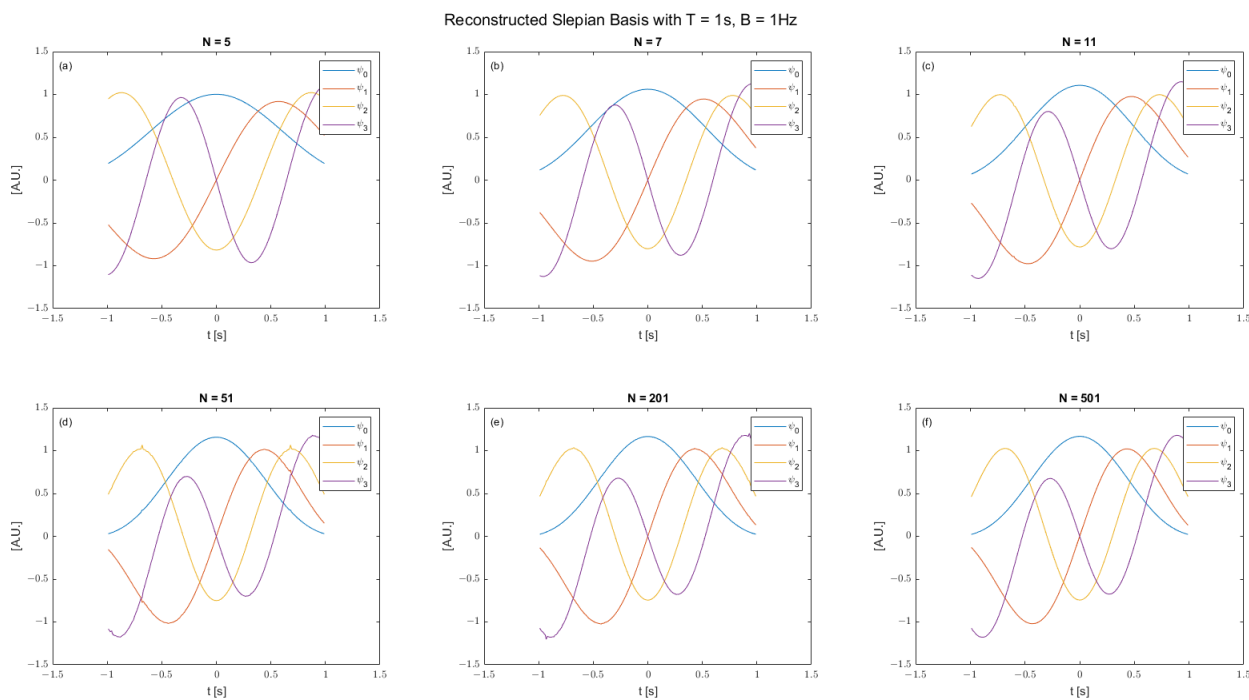


Figure 3. Reconstructed Slepian bases with different number of points N , (a–f) N from 5 to 501.

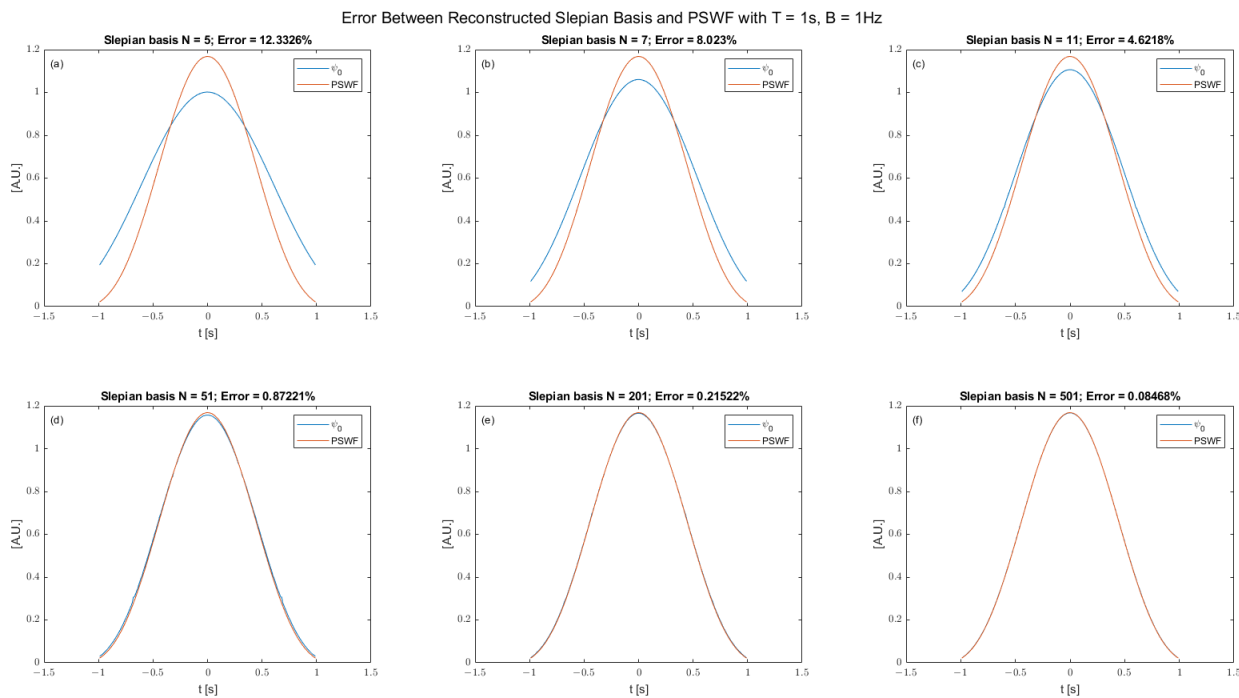


Figure 4. Error between sinc-series reconstructed Slepian bases with different N and PSWFs of order zero, (a–f) N from 5 to 501.

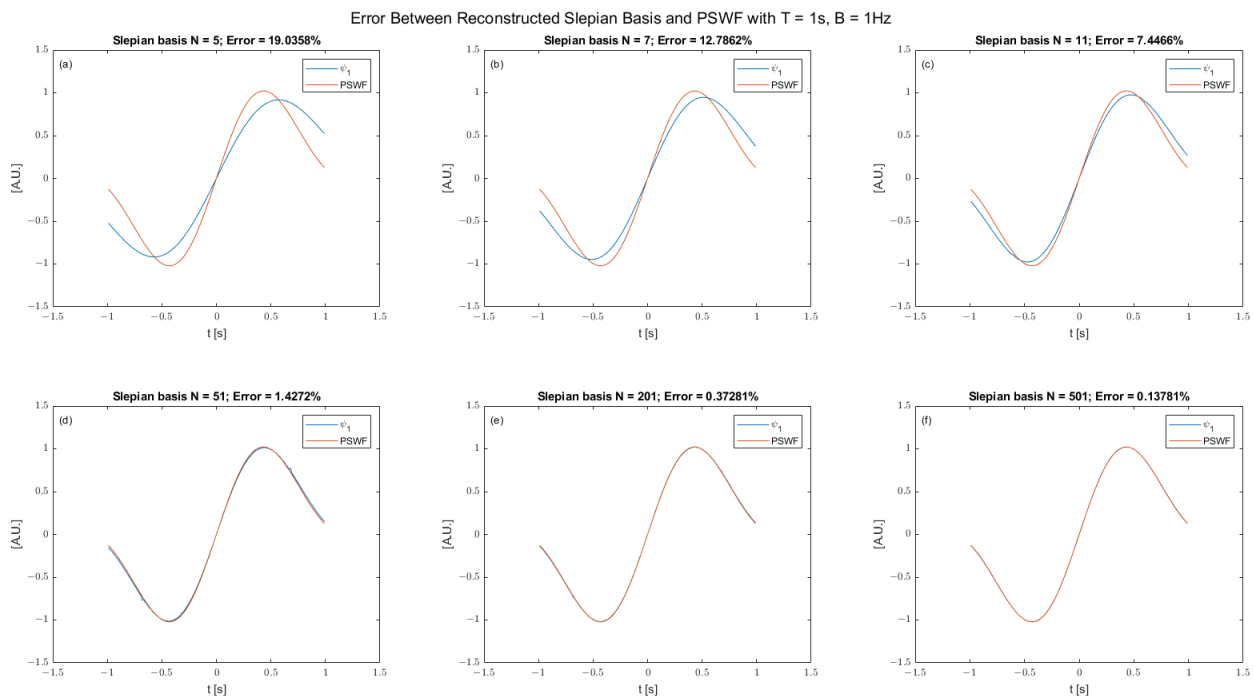


Figure 5. Error between sinc-series reconstructed Slepian bases with different N and PSWFs of order 1, (a–f) N from 5 to 501.

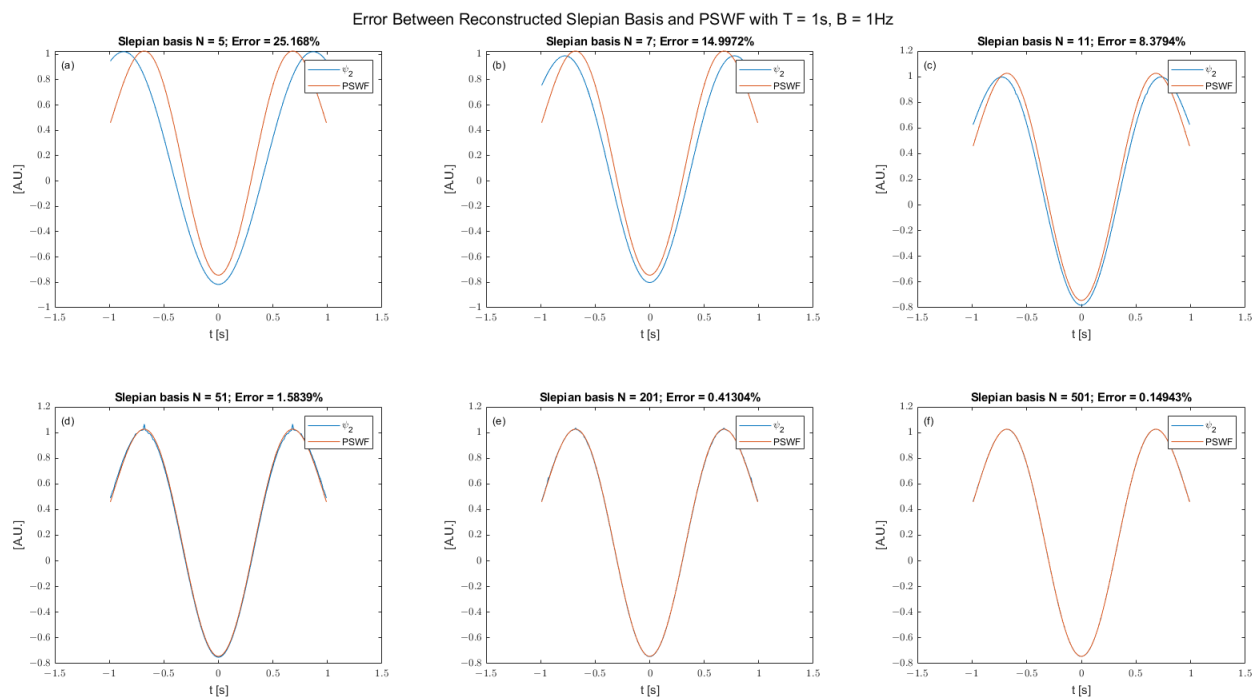


Figure 6. Error between sinc-series reconstructed Slepian bases with different N and PSWFs of order 2, (a–f) N from 5 to 501.

Figure 8 shows the trend observed in Figures 4–7 in a clearer manner as additional eigenvectors are generated and compared, using increasing values of N to evaluate the effect of N on error. In Figure 8, the duration and bandwidth of the eigenvectors are chosen to be $T = 1$ s and $B = 1.5915$ Hz, the minimum requirement for N is 7 points, and the eigenvectors obtained are of order from zero to six.

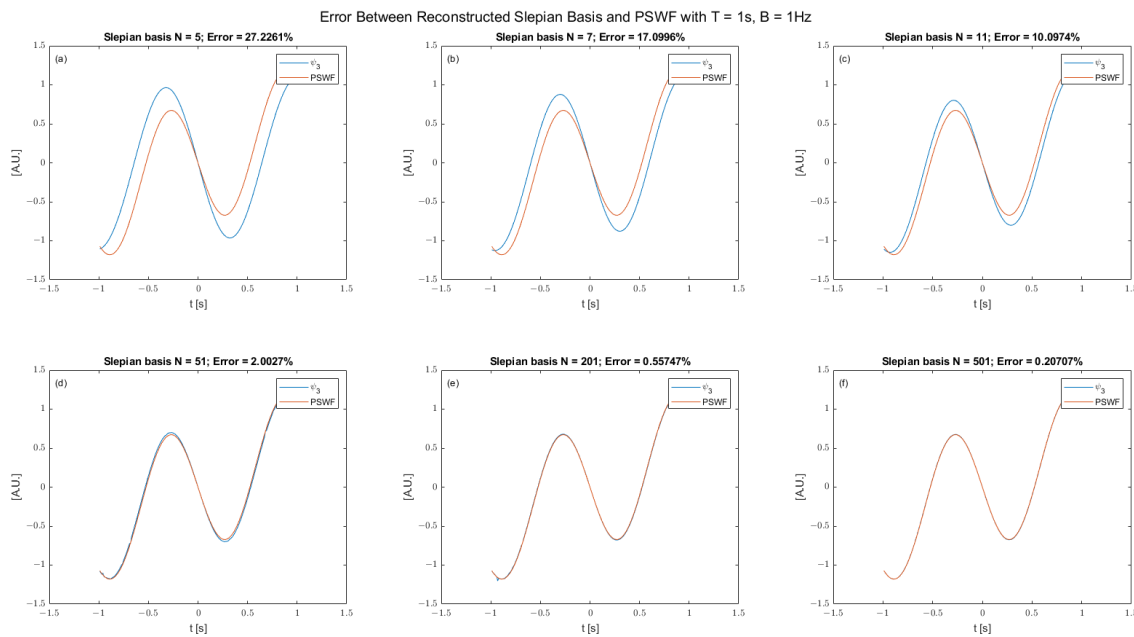


Figure 7. Error between sinc-series reconstructed Slepian bases with different N and PSWFs of order 3, (a–f) N from 5 to 501.

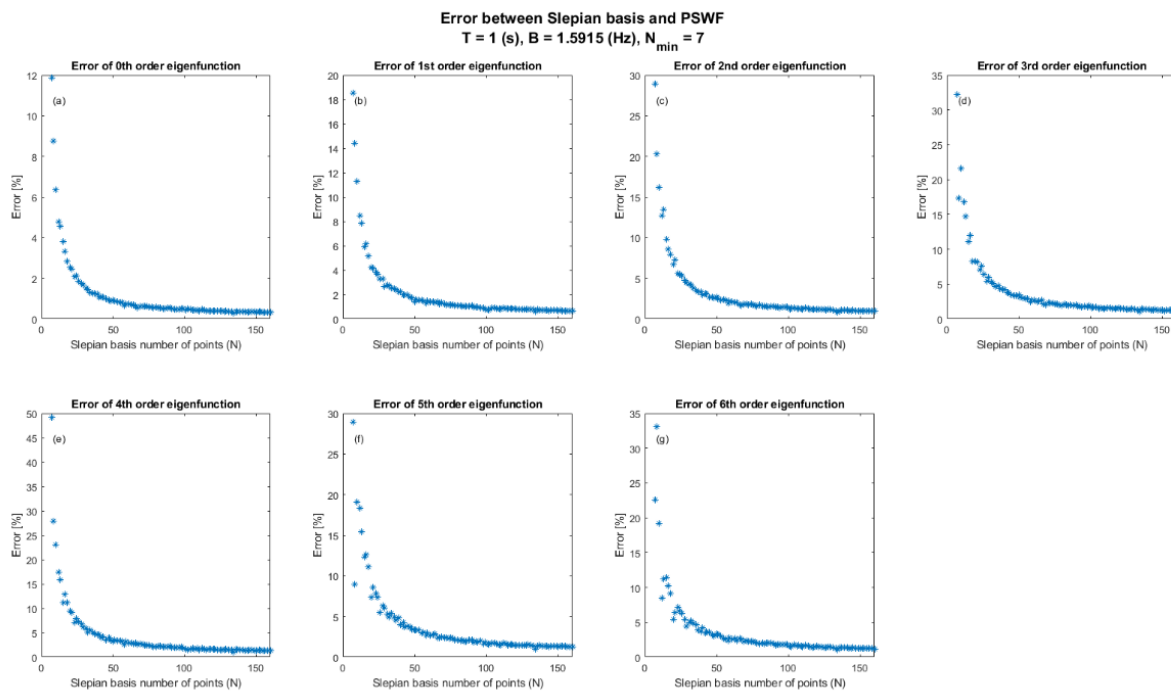


Figure 8. Eigenvector error vs. Slepian bases number of points, (a–g) shows the relation for different orders.

As can be seen from Figure 8, the error between eigenvectors decreases with increasing number of points. However, when the number of points, N , is sufficiently large enough, the gain in accuracy becomes small with increasing N . Thus, users need to balance between desired accuracy and the computational cost of increasing N . The same trend can also be observed with the error between eigenvalues shown in Figure 9, which shows the errors in eigenvectors of order 0 to 6 for increasing values of N . The errors between eigenvalues are calculated through Equation (48).

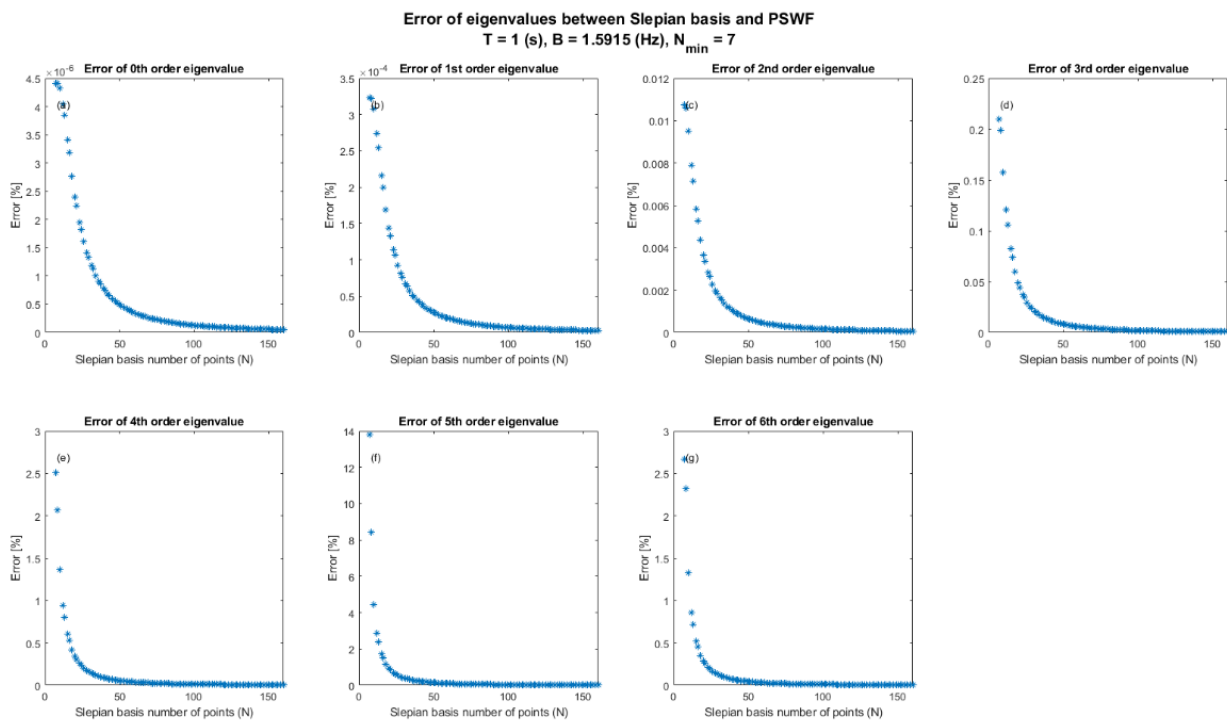


Figure 9. Eigenvalue error relation with number of points, for eigenvectors of order 0 to 6: (a–g) shows the relation for different orders.

To better illustrate that the error drops to low values when N is large enough, Figure 10 shows a curve fitting of the trends for the errors of the eigenvalues and eigenvectors of order zero with $c = 2\pi$. In Figure 10a,d, the errors in percentage for eigenvectors and eigenvalues are shown; Figure 10b,c are two different curve fitting methods for the errors of eigenvectors; Figure 10e,f are two different curve fitting methods for the errors of eigenvalues. Note that in Figure 10b,e, the vertical axes are the negative inverse of the percentage errors to show the decreasing pattern clearly. Curve fittings with other time-bandwidth products and orders can be found in Appendix B.

As can be seen in Figure 8, Figure 10, and the figures in Appendix B, the rate of error decreasing with the increasing number of points is different for different orders of the eigenvectors. Figure 11 provides a heuristic view of the error decrease rate by plotting the errors for different orders of eigenvectors in the same figure. Figure 11a shows the actual errors in percentages and the number on the legend is the order of the eigenvector. Figure 11b normalizes the errors to have the same maximum absolute value, so that the rate of error decrease can be observed more easily. PSWFs and Slepian are known to have the majority of their eigenvectors either close to 0 or close to 1, with a small number of eigenvectors falling in the ‘transition zone’ between 0 and 1. When the order of the eigenvector is in the ‘eigenvalue transition zone’, i.e., the associated eigenvalues are neither close to 1 nor close to zero, the errors are generally large and drop very slowly with increasing number of points.

However, fortunately for engineering applications, the eigenvectors with eigenvalue close to 1 are often the desired ones due to their compactness properties. Figure 12 calculates the mean error of eigenvectors with $c = 10$ but different orders and different number of points. For example, Figure 12a calculates the errors of 15 orders of eigenvectors with the same time-bandwidth product and same number of points. Then, a mean value of the 15 errors is shown on the subtitle of the subplot along with a mean value of the first $4TB$ order errors since it is known that there are $4TB$ eigenvalues close to 1 with a given time and bandwidth [51].

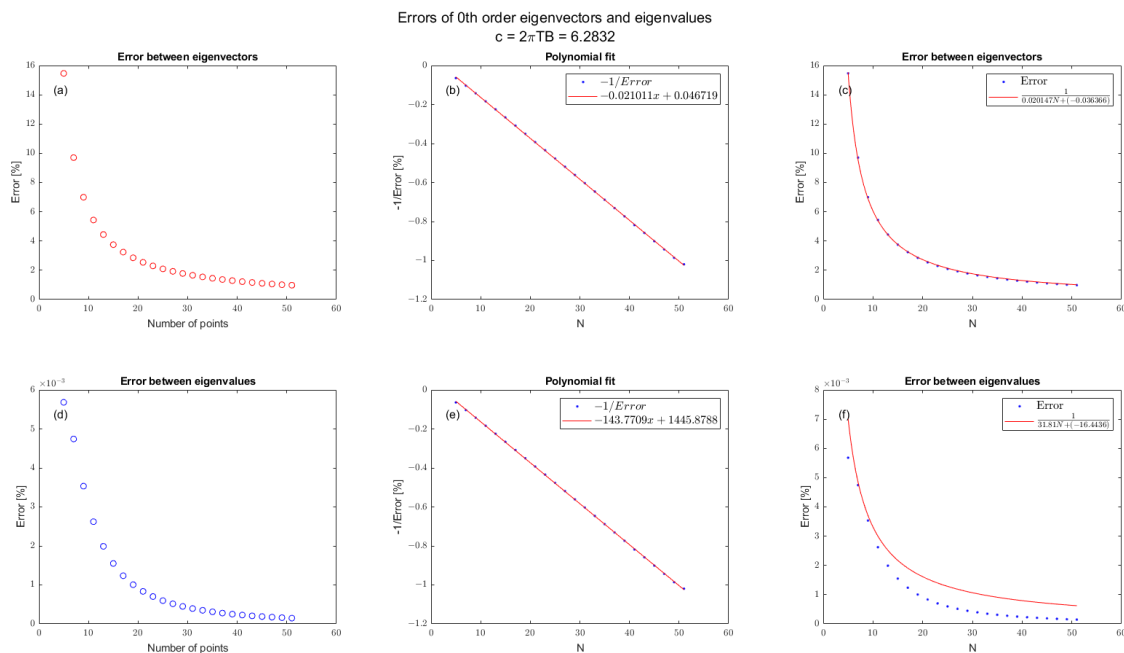


Figure 10. Error between reconstructed Slepian bases and PSWF of order zero with time-bandwidth product $c = 2\pi$: (a) error between eigenvectors; (b) linear curve fitting with vertical axis taken to be negative inverse of the error between eigenvectors; (c) parabolic curve fitting of the error between eigenvectors; (d) error between eigenvalues; (e) linear curve fitting with vertical axis taken to be negative inverse of the error between eigenvalues; (f) parabolic curve fitting of the error between eigenvalues.

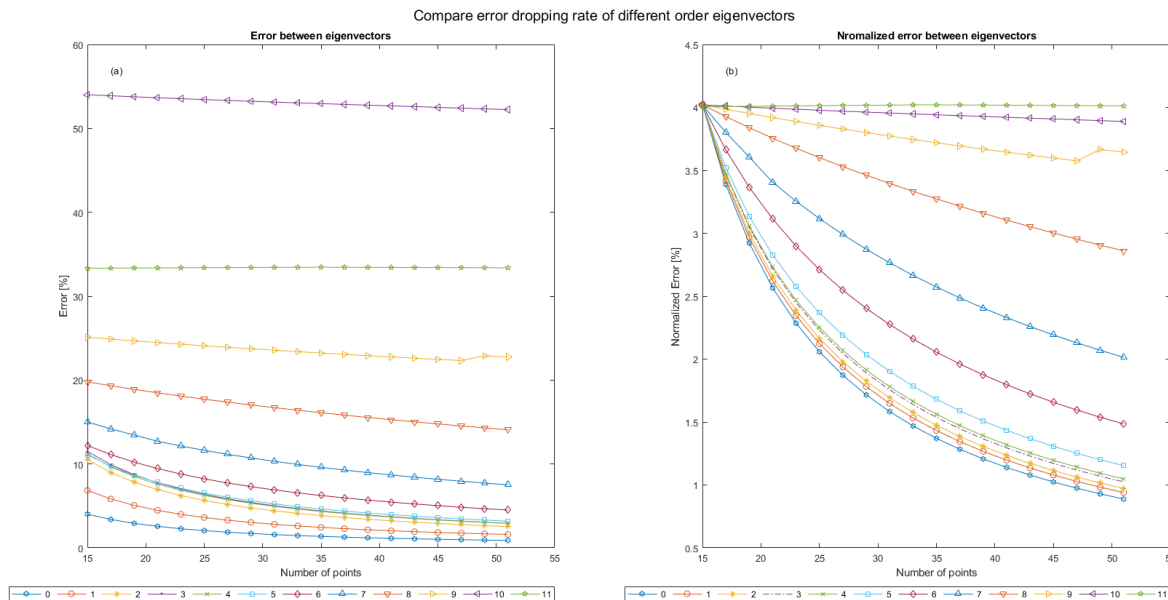


Figure 11. Comparison of rate of error decrease for different orders of eigenvectors.

As shown in Figure 12, the errors tend to be large with large orders of eigenvectors. However, the error within the first $4TB$ orders of eigenvectors are consistently small.

Another point of view from which to observe the error between the Slepian basis and PSWFs is through different time-bandwidth products. Simulations were used to determine the number of points required for the Slepian basis to reach less than 2% error between PSWFs for different time-bandwidth products (see Figure 13). Figure 13a shows the error when the Slepian basis reaches less than 2% error with the PSWF; Figure 13b shows the

number of points when the Slepian basis reaches less than 2% error for different time-bandwidth products (note here that the horizontal axis is taking “time-bandwidth products as TB for comparison with [50].”); Figure 13c,d show detailed plots of the vectors to provide a better view of how different they look from each other.

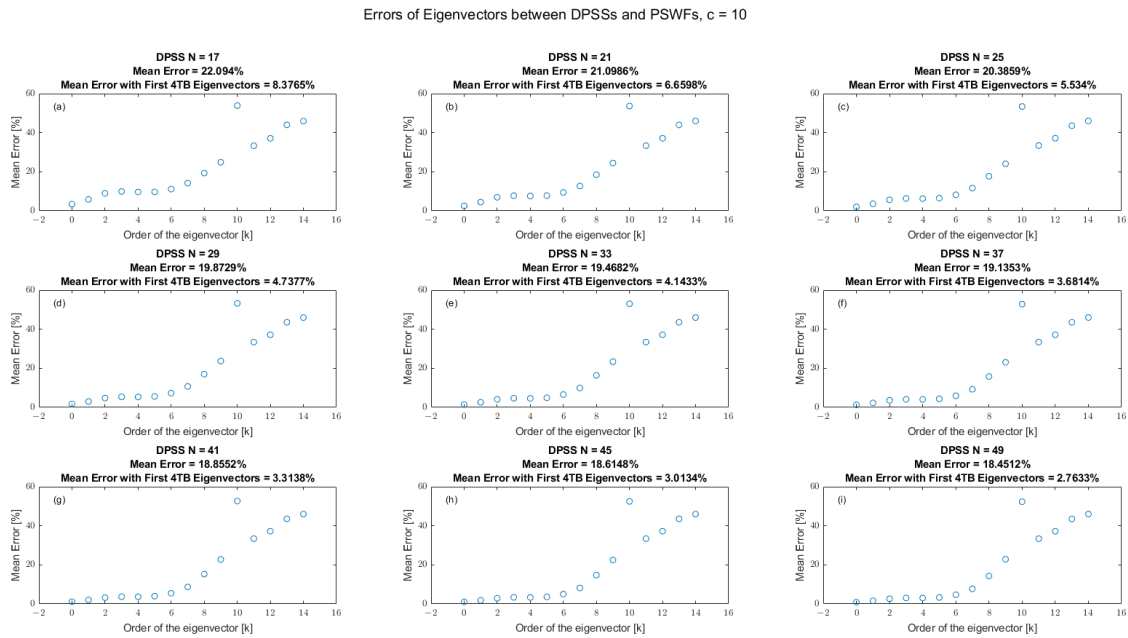


Figure 12. Error trend with orders of the eigenvectors: (a–i) N from 17 to 49.

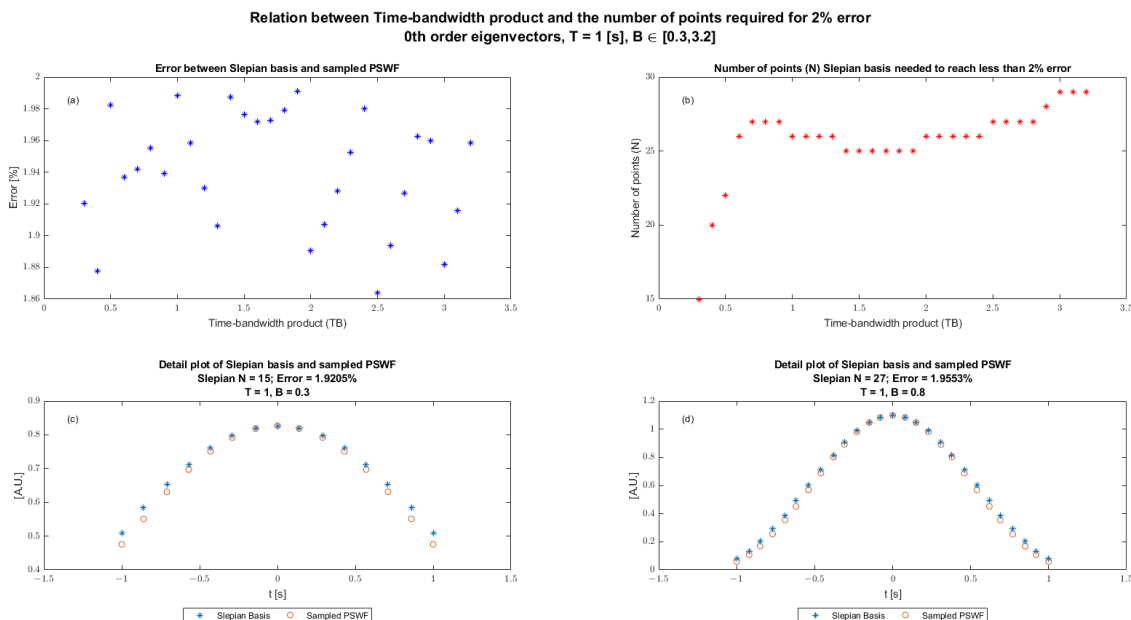


Figure 13. (a) Error between Slepian basis and PSWFs of order zero. (b) Number of points required to achieve less than 2% error against time-bandwidth products. (c) Detailed plot of Slepian basis with minimum N and PSWFs sampled at the same time. (d) Detailed plot of Slepian basis with larger N and PSWFs sampled at the same time.

In Figure 13, the duration of the vectors are kept the same as $T = 1$ s, while B ranges from 0.3 Hz to 3.2 Hz. The number of points in the Slepian basis needed to reach less than 2% error tends to be a constant value after a certain time-bandwidth threshold. In [50], it was shown that when TB of the Slepian basis of order zero is greater than a certain lower

threshold (approximately 0.5~1 depending on different measures used to define effective duration and bandwidth), the effective energy-based or variance-based time-bandwidth products tend to achieve a minimum value. Here, we demonstrate that a similar trend can also be observed with higher order eigenvectors, as shown in Figures 14 and 15.

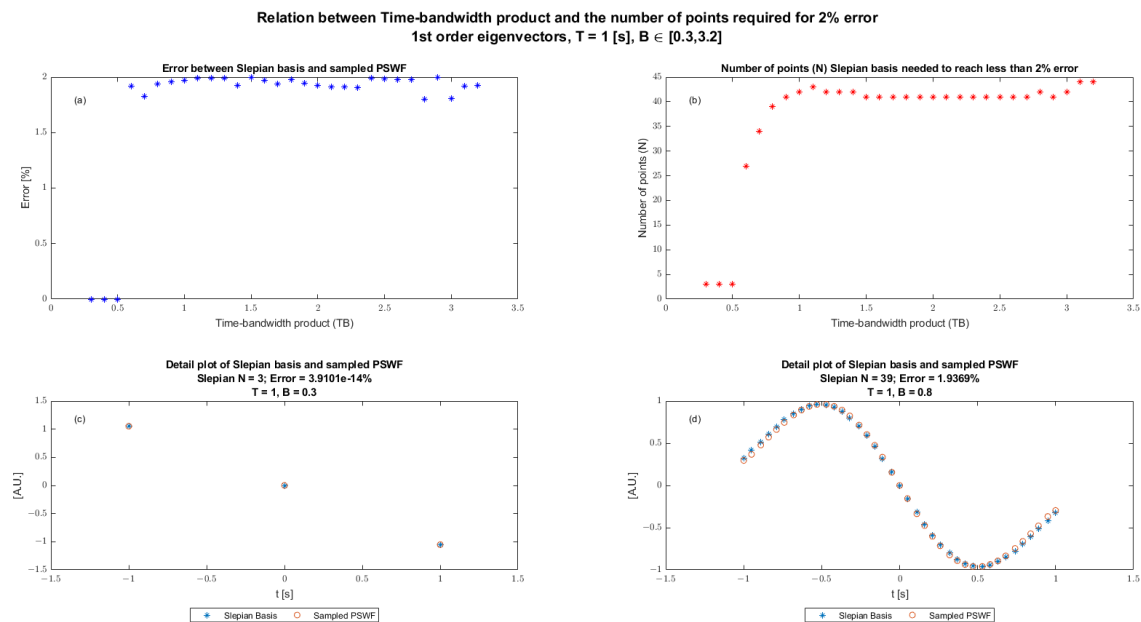


Figure 14. (a) Error between Slepian basis and PSWF of order one. (b) Number of points required to achieve less than 2% error versus time-bandwidth product. (c) Detailed plot of Slepian basis with minimum N and sampled PSWF values. (d) Detailed plot of Slepian basis with larger N and sampled PSWF values.

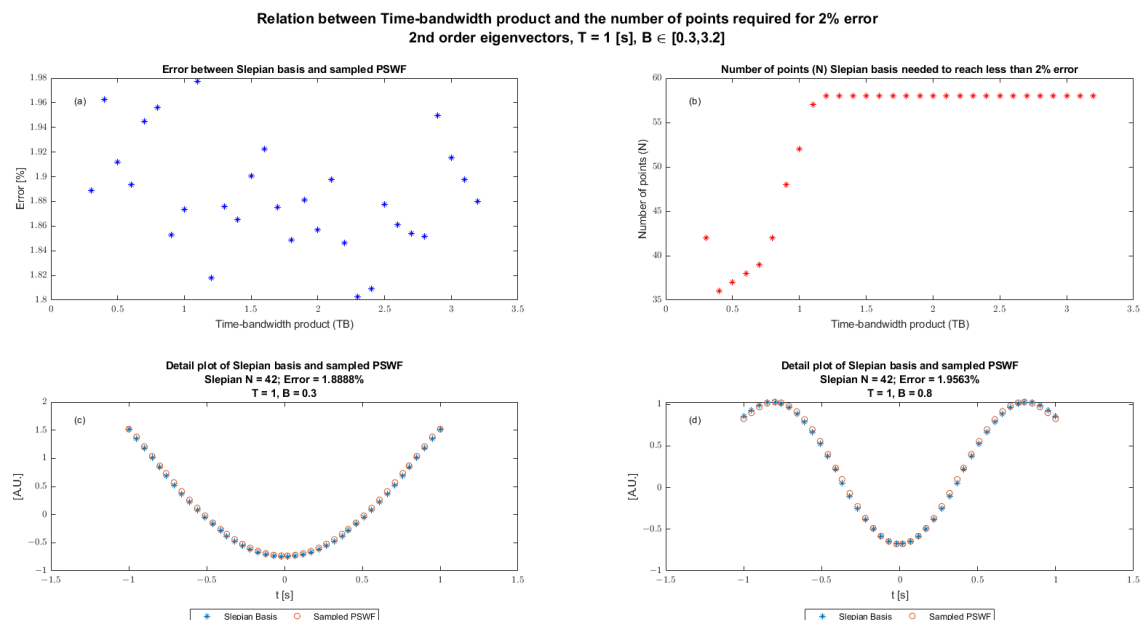


Figure 15. (a) Error between Slepian basis and PSWF of order two. (b) Number of points required to achieve less than 2% error against time-bandwidth products. (c) Detailed plot of Slepian basis with minimum N and sampled PSWF values. (d) Detailed plot of Slepian basis with larger N and sampled PSWF values.

Evaluating PSWFs with large time-bandwidth products ($c > 10$) is notoriously difficult [36]. In this section, we show that the PSWF can be evaluated with sinc-series reconstruction from the Slepian basis even with large time-bandwidth products. Figure 16 plots the zeroth order PSWFs and the reconstructed Slepian basis with different time-bandwidth products from (a) to (f). The errors are shown in the legends. PSWF_{Shannon} is the PSWF obtained through the Shannon sampling approach [35] and PSWF_{Quadrature} is the PSWF obtained through quadrature rules [20], to provide comparisons with our proposed reconstruction method.

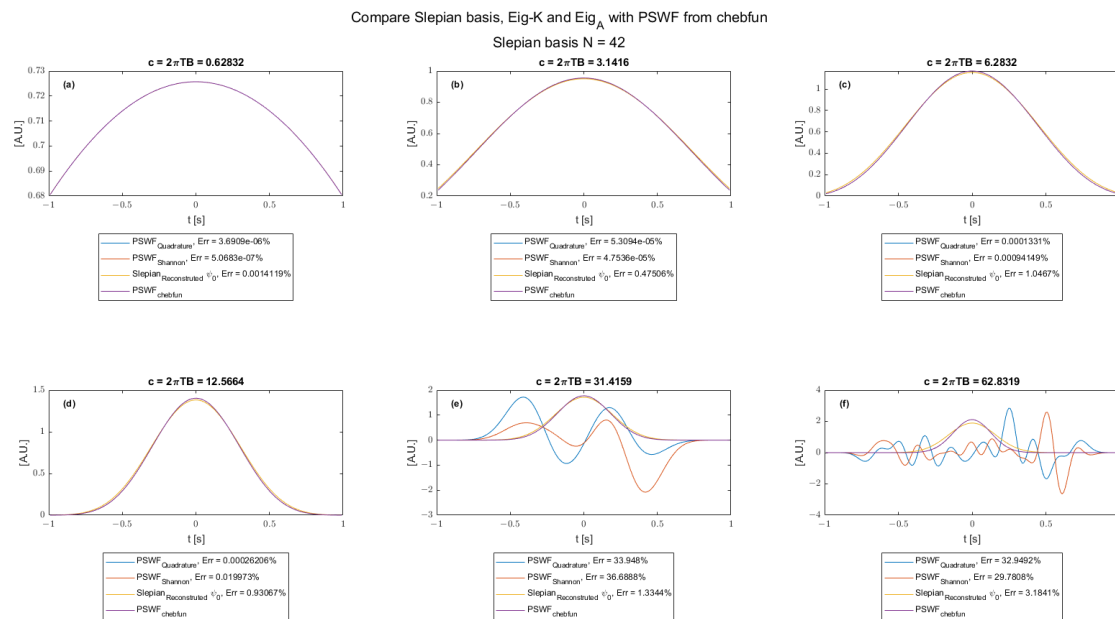


Figure 16. Errors between PSWFs generated with other methods and the proposed reconstructed Slepian basis approach, (a–f) c from 0.628 to 62.8.

As shown in Figure 16, the Shannon sampling approach and the quadrature method of evaluating PSWFs both start to fail when the time-bandwidth product increases, while the reconstructed Slepian basis as proposed in this paper still returns the true shape of PSWF and maintains small errors.

Furthermore, the run time for generating the plots in Figure 16 is recorded and shown in the legend of Figure 17. The run time for generating the Slepian basis without reconstruction is also provided.

As shown in Figure 17, the reconstructed Slepian basis method proposed in this paper uses less computational resources than the traditional quadrature or Shannon sampling approaches. In addition, if a continuous function is not required and using sampled values directly is acceptable (i.e., the reconstruction process can be omitted), then the run time for generating the sampled points of PSWFs can be shortened by another order of magnitude. Many vectorized applications require sampled function values. Our approach directly provides sampled values, which is a more efficient approach compared with producing continuous function approximations only to then sample them.

Although all the existing methods are fast (less than one second) to compute, for some applications the increase in computation efficiency still matters. For example, in photoacoustic imaging where PSWFs can be good candidates for input laser waveforms [52], a typical pulse repetition rate is 10 Hz [53,54]. This requires the calculation of the PSWF 10 times in one second. The traditional method of calculating PSWFs may not be implementable under such conditions.

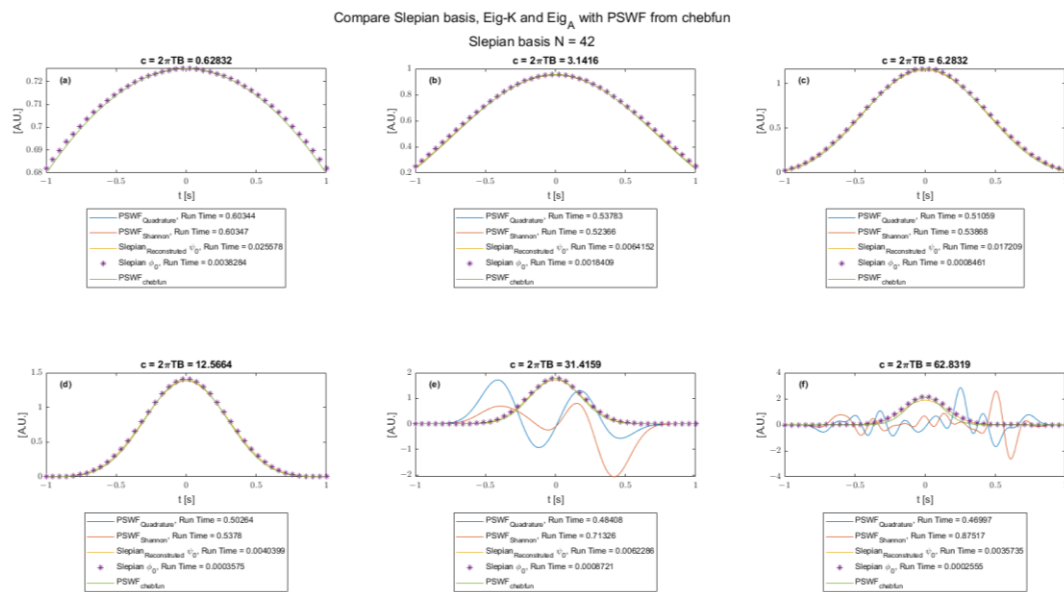


Figure 17. Run times of generating PSWFs using different approaches, (a–f) c from 0.628 to 62.8.

8. Summary and Conclusions

Computation of PSWFs is notoriously difficult and time consuming. This paper applies operator theory to discrete Fourier transform (DFT) to solve the problem of computing PSWFs. This leads to an infinite dimensional matrix operator eigenvalue problem, which we recognize as being the definition of the DPSSs. Truncation of the infinite matrix leads to a finite dimensional matrix eigenvalue problem which in turn yields what is known as the Slepian basis. These discrete-valued Slepian basis vectors can then be directly used as approximations of the discrete time evaluations of the PSWF, in other words, direct approximations to sampled values of the PSWF. Based on applying an inverse, Fourier transform demonstrates that a continuous PSWF can also be reconstructed from the Slepian-basis-sampled values of PSWF.

The simulation results discussed the feasibility of using reconstructed Slepian basis to evaluate the PSWFs with same time and bandwidth properties. The errors between the reconstructed Slepian basis and PSWFs are large when the orders of the eigenvectors are large. However, the errors within the first $4TB$ orders of eigenvectors whose eigenvalues are close to 1 are small. The accuracy can be increased by increasing the number of points used to generate the Slepian basis. The accuracy achieves an almost steady-state value where the rate of error decrease becomes small when the number of points is sufficiently large. Thus, users need to balance accuracy with computational costs. When increasing the time-bandwidth product of PSWFs, the number of Slepian basis points required for reconstruction to reach the same error level also increases. However, when the time-bandwidth product is increased to the value where maximum concentration is reached, the required number of points starts to remain constant. Furthermore, the method of reconstructing the Slepian basis can be more accurate (as shown in Figure 16) when compared to the Shannon sampling approach and quadrature approach for large time-bandwidth products. In addition, the method of reconstructing the Slepian basis is more efficient than the Shannon sampling approach and quadrature approach, as shown in Figure 17. Another result is that since the Slepian bases are approximately sampled values of PSWFs, when the number of points is large enough, the reconstruction process can be omitted entirely, as can be seen from Figure 2 with $N = 201$ and $N = 501$. The computational time can be reduced by an order of magnitude when the reconstruction process is omitted. However, when the number of points is small (as shown in Figure 14c), although the sampled points are sufficiently accurate, a sinc-series reconstruction is still needed to obtain the desired shape of the PSWF.

Author Contributions: Conceptualization, N.B.; funding acquisition, N.B.; investigation, Z.S.; resources, N.B.; software, Z.S.; validation, Z.S.; writing—original draft, Z.S.; writing—review and editing, N.B. All authors have read and agreed to the published version of the manuscript.

Funding: This research was funded by Natural Sciences and Engineering Research Council of Canada (NSERC), grant number RGPIN-2023-03392.

Data Availability Statement: Data are contained within the article.

Conflicts of Interest: The authors declare no conflict of interest. The funders had no role in the design of the study; in the collection, analyses, or interpretation of data; in the writing of the manuscript; or in the decision to publish the results.

Appendix A. Mathematical Definitions

Appendix A.1. The Fourier Transform

Let $L^2(\mathbb{R}) \triangleq L^2(-\infty, \infty)$ be the space of square integrable functions $f(r)$ on the real line $r \in (-\infty, \infty)$ with the inner product defined as [44]

$$\langle f, g \rangle = \int_{-\infty}^{\infty} f(t) \overline{g(t)} dt \quad (\text{A1})$$

Here, the overbar indicates the complex conjugate operation. This inner product induces a norm

$$\|f\| = \langle f, f \rangle^{1/2} = \left(\int_{-\infty}^{\infty} |f(t)|^2 dt \right)^{1/2} \quad (\text{A2})$$

In signal processing terms, the energy of the signal is typically defined as $E_f = \langle f, f \rangle = \|f\|^2$.

The Fourier transform of a function $f(t)$ is defined as a linear operator on $L^2(\mathbb{R})$ by the integral

$$F(\omega) = \mathbb{F}[f](\omega) = \mathbb{F}[f(t)] = \int_{-\infty}^{\infty} f(t) e^{-i\omega t} dt = \langle f(t), e^{i\omega t} \rangle \quad (\text{A3})$$

The Fourier transform transforms functions in the spatial variable t to functions in the angular frequency ω domain such that $f(t) \Leftrightarrow F(\omega)$. The notation \Leftrightarrow is used to indicate a Fourier transform pair. Here, we use the capitalization to denote a Fourier transform (F is the Fourier transform of the function f).

An integral transform needs to be invertible in order to be useful. The inversion formula is given by

$$f(t) = \mathbb{F}^{-1}[F](t) = \mathbb{F}^{-1}[F(\omega)] = \frac{1}{2\pi} \int_{-\infty}^{\infty} F(\omega) e^{i\omega t} d\omega = \frac{1}{2\pi} \langle F(\omega), e^{-i\omega t} \rangle \quad (\text{A4})$$

Appendix A.2. Parseval Relation

The functions belonging to $L^2(\mathbb{R})$ satisfy the generalized Parseval relation [44]:

$$\int_{-\infty}^{\infty} f(t) \overline{g(t)} dt = \frac{1}{2\pi} \int_{-\infty}^{\infty} F(\omega) \overline{G(\omega)} d\omega \quad (\text{A5})$$

This can be written as

$$\langle f, g \rangle = \frac{1}{2\pi} \langle F, G \rangle \quad (\text{A6})$$

This also yields the useful observation that the energy of a signal/function can be equivalently calculated in either the time or frequency domain, that is

$$\langle f, f \rangle = \frac{1}{2\pi} \langle F, F \rangle \quad (\text{A7})$$

Appendix B. Curve Fitting for Relation between Error and Slepian Basis Number of Points

This appendix provides the curve fitting for relation between errors and the Slepian basis number of points. Figures A1 and A2 show the errors in the eigenvectors and eigenvalues between the reconstructed Slepian basis and PSWF with $c = 1$ of order 0 and order 1, respectively.

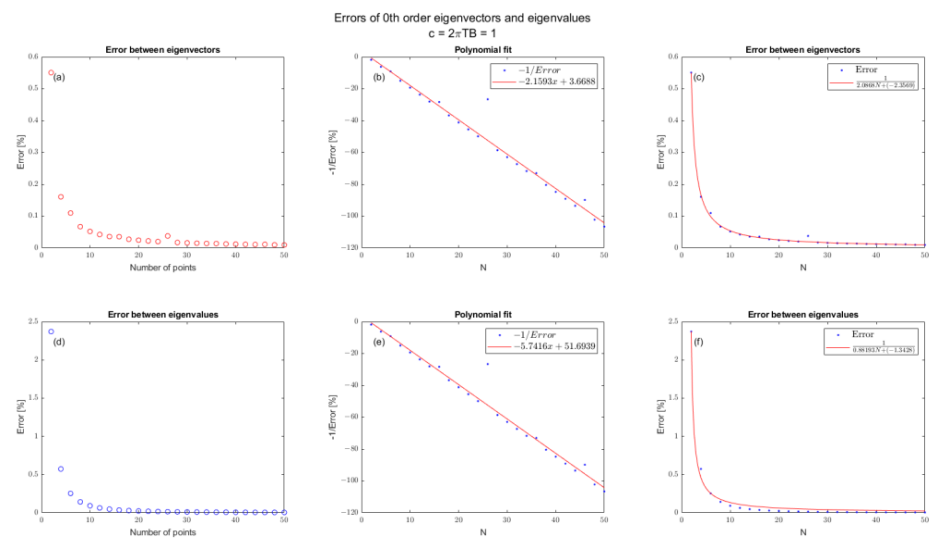


Figure A1. Error between reconstructed Slepian basis and PSWF of order zero with time-bandwidth product $c = 1$; (a) error between eigenvectors; (b) linear curve fitting with vertical axis taken to be negative inverse of the error between eigenvectors; (c) parabolic curve fitting of the error between eigenvectors; (d) error between eigenvalues; (e) linear curve fitting with vertical axis taken to be negative inverse of the error between eigenvalues; (f) parabolic curve fitting of the error between eigenvalues.

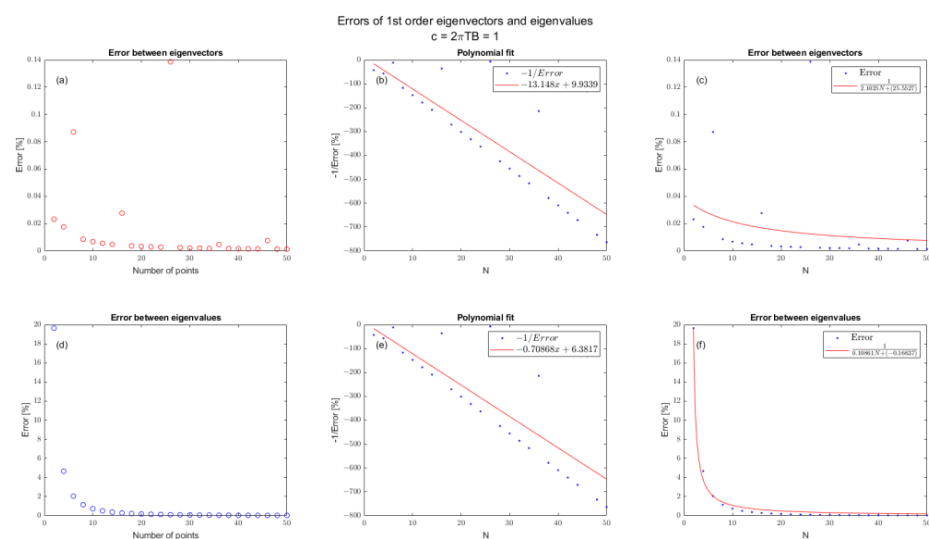


Figure A2. Error between reconstructed Slepian basis and PSWF of order one with time-bandwidth product $c = 1$; (a) error between eigenvectors; (b) linear curve fitting with vertical axis taken to be

negative inverse of the error between eigenvectors; (c) parabolic curve fitting of the error between eigenvectors; (d) error between eigenvalues; (e) linear curve fitting with vertical axis taken to be negative inverse of the error between eigenvalues; (f) parabolic curve fitting of the error between eigenvalues.

References

1. Slepian, D.; Pollak, H.O. Prolate Spheroidal Wave Functions, Fourier Analysis and Uncertainty—I. *Bell Syst. Tech. J.* **1961**, *40*, 43–63. [\[CrossRef\]](#)
2. Landau, H.J.; Pollak, H.O. Prolate Spheroidal Wave Functions, Fourier Analysis and Uncertainty—II. *Bell Syst. Tech. J.* **1961**, *40*, 65–84. [\[CrossRef\]](#)
3. Landau, H.J.; Pollak, H.O. Prolate Spheroidal Wave Functions, Fourier Analysis and Uncertainty—III: The Dimension of the Space of Essentially Time- and Band-Limited Signals. *Bell Syst. Tech. J.* **1962**, *41*, 1295–1336. [\[CrossRef\]](#)
4. Slepian, D. Prolate Spheroidal Wave Functions, Fourier Analysis and Uncertainty—IV: Extensions to Many Dimensions; Generalized Prolate Spheroidal Functions. *Bell Syst. Tech. J.* **1964**, *43*, 3009–3057. [\[CrossRef\]](#)
5. Slepian, D. Prolate Spheroidal Wave Functions, Fourier Analysis, and Uncertainty—V: The Discrete Case. *Bell Syst. Tech. J.* **1978**, *57*, 1371–1430. [\[CrossRef\]](#)
6. Noorishad, P.; Yatawatta, S. Efficient computation of prolate spheroidal wave functions in radio astronomical source modeling. In Proceedings of the 2011 IEEE International Symposium on Signal Processing and Information Technology (ISSPIT), Bilbao, Spain, 14–17 December 2011; pp. 326–330.
7. Takami, T.; Nielsen, U.D.; Jensen, J.J. Application of prolate spheroidal wave functions for assessment and prediction of ship responses. In Proceedings of the 15th International Symposium on Practical Design of Ships and Other Floating Structures, Dubrovnik, Croatia, 9–13 October 2022.
8. Takami, T.; Nielsen, U.D.; Xi, C.; Jensen, J.J.; Oka, M. Reconstruction of Incident Wave Profiles Based on Short-Time Ship Response Measurements. *Appl. Ocean Res.* **2022**, *123*, 103183. [\[CrossRef\]](#)
9. Gonzalez, M.C. Engineering Applications of Prolate Spheroidal Wave Functions and Sequences and Legendre Polynomials: Filtering and Beamforming in 1D and 2D. Ph.D. Thesis, University of California, Davis, CA, USA, 2018.
10. Yang, Q.X.; Lindquist, M.A.; Shepp, L.; Zhang, C.-H.; Wang, J.; Smith, M.B. Two Dimensional Prolate Spheroidal Wave Functions for MRI. *J. Magn. Reson.* **2002**, *158*, 43–51. [\[CrossRef\]](#)
11. Dullaert, W.; Reichardt, L.; Rogier, H. Improved Detection Scheme for Chipless RFIDs Using Prolate Spheroidal Wave Function-Based Noise Filtering. *IEEE Antennas Wirel. Propag. Lett.* **2011**, *10*, 472–475. [\[CrossRef\]](#)
12. Chen, Z.; Wang, H.; Liu, X.; Zhong, P. Maximal Capacity Nonorthogonal Pulse Shape Modulation. *Chin. J. Aeronaut.* **2015**, *28*, 1699–1708. [\[CrossRef\]](#)
13. Tang, W.-G.; Jiang, H.; Zhang, Q.; Jiang, H. PSWF-Based Decoupled Atomic Norm Minimization for DOD and DOA Estimation in MIMO Radar with Arbitrary Linear Arrays. *Signal Process.* **2023**, *212*, 109136. [\[CrossRef\]](#)
14. Beck, F.C.; Enneking, C.; Thölert, S.; Antreich, F. Comparison of constant and non-constant envelope signals for satellite navigation. In Proceedings of the 2022 10th Workshop on Satellite Navigation Technology (NAVITEC), Noordwijk, The Netherlands, 5–7 April 2022; pp. 1–9.
15. Van Hoorickx, C.; Reynders, E.P.B. Numerical Realization of Diffuse Sound Pressure Fields Using Prolate Spheroidal Wave Functions. *J. Acoust. Soc. Am.* **2022**, *151*, 1710–1721. [\[CrossRef\]](#)
16. Slepian, D. Some Comments on Fourier Analysis, Uncertainty and Modeling. *SIAM Rev.* **1983**, *25*, 379–393. [\[CrossRef\]](#)
17. Boyd, J.P. Algorithm 840: Computation of Grid Points, Quadrature Weights and Derivatives for Spectral Element Methods Using Prolate Spheroidal Wave Functions—Prolate Elements. *ACM Trans. Math. Softw.* **2005**, *31*, 149–165. [\[CrossRef\]](#)
18. Schmutzhard, S.; Hrycak, T.; Feichtinger, H.G. A Numerical Study of the Legendre-Galerkin Method for the Evaluation of the Prolate Spheroidal Wave Functions. *Numer. Algorithms* **2015**, *68*, 691–710. [\[CrossRef\]](#)
19. Osipov, A.; Rokhlin, V. On the Evaluation of Prolate Spheroidal Wave Functions and Associated Quadrature Rules. *Appl. Comput. Harmon. Anal.* **2014**, *36*, 108–142. [\[CrossRef\]](#)
20. Xiao, H.; Rokhlin, V.; Yarvin, N. Prolate Spheroidal Wavefunctions, Quadrature and Interpolation. *Inverse Probl.* **2001**, *17*, 805. [\[CrossRef\]](#)
21. Bouwkamp, C.J. On Spheroidal Wave Functions of Order Zero. *J. Math. Phys.* **1947**, *26*, 79–92. [\[CrossRef\]](#)
22. Karoui, A.; Moumni, T. New Efficient Methods of Computing the Prolate Spheroidal Wave Functions and Their Corresponding Eigenvalues. *Appl. Comput. Harmon. Anal.* **2008**, *24*, 269–289. [\[CrossRef\]](#)
23. Bonami, A.; Karoui, A. Uniform Approximation and Explicit Estimates for the Prolate Spheroidal Wave Functions. *Constr. Approx.* **2016**, *43*, 15–45. [\[CrossRef\]](#)
24. Falloon, P.E.; Abbott, P.C.; Wang, J.B. Theory and Computation of Spheroidal Wavefunctions. *J. Phys. A Math. Gen.* **2003**, *36*, 5477. [\[CrossRef\]](#)
25. Osipov, A. Certain Upper Bounds on the Eigenvalues Associated with Prolate Spheroidal Wave Functions. *Appl. Comput. Harmon. Anal.* **2013**, *35*, 309–340. [\[CrossRef\]](#)

26. Rokhlin, V.; Xiao, H. Approximate Formulae for Certain Prolate Spheroidal Wave Functions Valid for Large Values of Both Order and Band-Limit. *Appl. Comput. Harmon. Anal.* **2007**, *22*, 105–123. [[CrossRef](#)]
27. Hodge, D.B. Eigenvalues and Eigenfunctions of the Spheroidal Wave Equation. *J. Math. Phys.* **1970**, *11*, 2308–2312. [[CrossRef](#)]
28. Adelman, R.; Gumerov, N.A.; Duraiswami, R. Software for Computing the Spheroidal Wave Functions Using Arbitrary Precision Arithmetic. *arXiv* **2014**, arXiv:1408.0074.
29. Kirby, P. Calculation of Spheroidal Wave Functions. *Comput. Phys. Commun.* **2006**, *175*, 465–472. [[CrossRef](#)]
30. Rehan, R.; Bremer, J. An O(1) Algorithm for the Numerical Evaluation of the Sturm-Liouville Eigenvalues of the Spheroidal Wave Functions of Order Zero. *Appl. Comput. Harmon. Anal.* **2022**, *60*, 1–19. [[CrossRef](#)]
31. Alici, H.; Shen, J. Highly Accurate Pseudospectral Approximations of the Prolate Spheroidal Wave Equation for Any Bandwidth Parameter and Zonal Wavenumber. *J. Sci. Comput.* **2017**, *71*, 804–821. [[CrossRef](#)]
32. Huang, Z.; Xiao, J.; Boyd, J.P. Adaptive Radial Basis Function and Hermite Function Pseudospectral Methods for Computing Eigenvalues of the Prolate Spheroidal Wave Equation for Very Large Bandwidth Parameter. *J. Comput. Phys.* **2015**, *281*, 269–284. [[CrossRef](#)]
33. Bremer, J. On the Numerical Evaluation of the Prolate Spheroidal Wave Functions of Order Zero. *Appl. Comput. Harmon. Anal.* **2022**, *60*, 53–76. [[CrossRef](#)]
34. Osipov, A.; Rokhlin, V.; Xiao, H. *Prolate Spheroidal Wave Functions of Order Zero: Mathematical Tools for Bandlimited Approximation*, 2013rd ed.; Springer: Berlin/Heidelberg, Germany, 2013.
35. Khare, K.; George, N. Sampling Theory Approach to Prolate Spheroidal Wavefunctions. *J. Phys. A Math. Gen.* **2003**, *36*, 10011. [[CrossRef](#)]
36. Walter, G.; Soleski, T. A New Friendly Method of Computing Prolate Spheroidal Wave Functions and Wavelets. *Appl. Comput. Harmon. Anal.* **2005**, *19*, 432–443. [[CrossRef](#)]
37. Walter, G.G.; Shen, X. Recovery of digitized signals using Slepian functions. In Proceedings of the 2003 IEEE International Conference on Acoustics, Speech, and Signal Processing, Proceedings. (ICASSP '03), Hong Kong, China, 6–10 April 2003; Volume 6, p. VI-241.
38. Walter, G.G.; Shen, X.A. Sampling with Prolate Spheroidal Wave Functions. *Sampl. Theory Signal Image Process.* **2003**, *2*, 25–52. [[CrossRef](#)]
39. Hogan, J.A.; Izu, S.; Lakey, J.D. Sampling Approximations for Time- and Bandlimiting. *Sampl. Theory Signal Image Process.* **2010**, *9*, 91–117. [[CrossRef](#)]
40. Çiçek, H.; Zainalabdin, S.J.; İzgi, A. A New Generalization of Szasz-Kantorovich Operators on Weighted Space. *Turk. J. Sci.* **2022**, *7*, 85–106.
41. Aksoy, N.Y.; Sarıahmet, E. On the Stability of Finite Difference Scheme for the Schrödinger Equation Including Momentum Operator. *Turk. J. Sci.* **2022**, *7*, 107–115.
42. Pankov, P.S.; Zheentaeva, Z.K.; Shirinov, T. Asymptotic reduction of solution space dimension for dynamical systems. *TWMS J. Pure Appl. Math.* **2021**, *12*, 243–253.
43. Kennedy, R.A.; Sadeghi, P. *Hilbert Space Methods in Signal Processing*, Illustrated ed.; Cambridge University Press: Cambridge, UK, 2013; ISBN 978-1-107-01003-1.
44. Howell, K. Fourier Transforms. In *The Transforms and Applications Handbook*; CRC Press LLC: Boca Raton, FL, USA, 2000; Volume 2, pp. 2.1–2.159.
45. Khare, K.; Butola, M.; Rajora, S. Sampling Theorem. In *Fourier Optics and Computational Imaging*; Khare, K., Butola, M., Rajora, S., Eds.; Springer International Publishing: Cham, The Netherlands, 2023; pp. 33–49. ISBN 978-3-031-18353-9.
46. Unser, M. Sampling-50 Years after Shannon. *Proc. IEEE* **2000**, *88*, 569–587. [[CrossRef](#)]
47. Breitenberger, E. SSA Matlab Implementation; 1995.
48. Driscoll, T.; Hale, N.; Trefethen, L. *Chebfun Guide*; Pafnuty Publications: Oxford, UK, 2014.
49. Flammer, C. *Spheroidal Wave Functions*; Stanford Research Institute Monograph; Stanford University Press: Stanford, CA, USA, 1957.
50. Sun, Z.; Baddour, N. On the Time Frequency Compactness of the Slepian Basis of Order Zero for Engineering Applications. *Computation* **2023**, *11*, 116. [[CrossRef](#)]
51. Karnik, S.; Romberg, J.; Davenport, M.A. Improved Bounds for the Eigenvalues of Prolate Spheroidal Wave Functions and Discrete Prolate Spheroidal Sequences. *Appl. Comput. Harmon. Anal.* **2021**, *55*, 97–128. [[CrossRef](#)]
52. Baddour, N.; Sun, Z. Photoacoustics Waveform Design for Optimal Signal to Noise Ratio. *Symmetry* **2022**, *14*, 2233. [[CrossRef](#)]
53. Mao, Q.; Zhao, W.; Qian, X.; Tao, C.; Liu, X. Improving Photoacoustic Imaging in Low Signal-to-Noise Ratio by Using Spatial and Polarity Coherence. *Photoacoustics* **2022**, *28*, 100427. [[CrossRef](#)]
54. Oh, J.-T.; Li, M.-L.; Zhang, H.F.; Maslov, K.; Wang, L.V. Three-Dimensional Imaging of Skin Melanoma in Vivo by Dual-Wavelength Photoacoustic Microscopy. *J. Biomed. Opt.* **2006**, *11*, 034032. [[CrossRef](#)]

Disclaimer/Publisher's Note: The statements, opinions and data contained in all publications are solely those of the individual author(s) and contributor(s) and not of MDPI and/or the editor(s). MDPI and/or the editor(s) disclaim responsibility for any injury to people or property resulting from any ideas, methods, instructions or products referred to in the content.